DEVELOPMENT OF A PORTABLE NEUTRON COINCIDENCE COUNTER FOR FIELD MEASUREMENTS OF NUCLEAR MATERIALS USING THE ADVANCED MULTIPLICITY CAPABILITIES OF MCNPX 2.5.F AND THE NEUTRON COINCIDENCE POINT MODEL

A Thesis

by

ANGELA LYNN THORNTON

Submitted to the Office of Graduate Studies of
Texas A&M University
in partial fulfillment of the requirements for the degree of

MASTER OF SCIENCE

December 2007

Major Subject: Nuclear Engineering

DEVELOPMENT OF A PORTABLE NEUTRON COINCIDENCE COUNTER FOR FIELD MEASUREMENTS OF NUCLEAR MATERIALS USING THE ADVANCED MULTIPLICITY CAPABILITIES OF MCNPX 2.5.F AND THE NEUTRON COINCIDENCE POINT MODEL

A Thesis

by

ANGELA LYNN THORNTON

Submitted to the Office of Graduate Studies of
Texas A&M University
in partial fulfillment of the requirements for the degree of

MASTER OF SCIENCE

Approved by:

Chair of Committee,	William Charlton
Committee Members,	Paul Nelson
	Arnold Vedlitz
Head of Department,	Raymond Juzaitis

December 2007

Major Subject: Nuclear Engineering

ABSTRACT

Development of a Portable Neutron Coincidence Counter for Field Measurements of Nuclear Materials Using the Advanced Multiplicity Capabilities of MCNPX 2.5.F and the Neutron Coincidence Point Model. (December 2007)

Angela Lynn Thornton, B.S., Texas A&M University;

M.S., Texas A&M University

Chair of Advisory Committee: Dr. William Charlton

Neutron coincidence counting is an important passive Nondestructive Assay (NDA) technique widely used for qualitative and quantitative analysis of nuclear material in bulk samples. During the fission process, multiple neutrons are simultaneously emitted from the splitting nucleus. These neutron groups are often referred to as coincident neutrons. Because different isotopes possess different coincident neutron characteristics, the coincident neutron signature can be used to identify and quantify a given material. In an effort to identify unknown nuclear samples in field inspections, the Portable Neutron Coincidence Counter (PNCC) has been developed. This detector makes use of the coincident neutrons being emitted from a bulk sample. An in-depth analysis has been performed to establish whether the nuclear material in an unknown sample could be quantified with the accuracy and precision needed for safeguards measurements. The analysis was performed by comparing experimental measurements of PuO_2 samples to the calculated output produced using MCNPX and the Neutron Coincidence Point Model. Based on the analysis, it is evident that this new portable system can play a useful role in identifying nuclear material for verification purposes.

ACKNOWLEDGEMENTS

This research is the result of the efforts of many individuals to whom I owe the utmost appreciation. I must first sincerely thank my research chair, Dr. Bill Charlton. Dr. Charlton has guided me over the long duration of my research. His patience throughout is not only a sign of wisdom, but is a reflection upon his character. Without his expertise, I would have been lost. I also extend sincere gratitude to the members of my committee, Dr. Paul Nelson and Dr. Arnie Vedlitz for their valuable input.

I would also like to thank Los Alamos National Laboratory for the opportunity to work on this project. It was with the help of the Howard Menlove, Mike Miller, Martyn Swinhoe, and Carlos Rael, and other N-1 Safeguards Science and Technology staff that I was able to achieve the goals of this research.

NOMENCLATURE

IAEA	International Atomic Energy Agency
NDA	Non-Destructive Analysis
LANL	Los Alamos National Laboratory
PNCC	Portable Neutron Coincidence Counter
MCNPX	Monte Carlo N- Particle (eXtended) code
HLNCC	High Level Neutron Coincidence Counter
AWCC	Active Well Coincidence Counter
CPS	Counts per second
INCC	IAEA Neutron Coincidence Counting software
LAO	Los Alamos Operations
FFTF	Fast Flux Test Facility
MOX	Mixed-oxide

TABLE OF CONTENTS

LIST OF TABLES

TABLE Page

LIST OF FIGURES

FIGURE Page

CHAPTER I

INTRODUCTION

MOTIVATION AND OBJECTIVES

Imagine you are a nuclear safeguards inspector for the International Atomic Energy Agency (IAEA) and have been assigned the difficult task of verifying the nuclear declarations of a suspicious facility in a rogue country. As if not already difficult enough, your job can be complicated by numerous other factors such as false declarations, modified samples, hidden materials, limited access, and other environmental factors. Ideally you would like to perform some type of non-destructive assay (NDA) on various samples in the facility to verify the nuclear material inside. One of the most frequently used techniques for this application is neutron coincidence counting.

Determining the total mass of nuclear material is the main objective in most neutron coincidence measurement applications. More specifically, IAEA inspectors often rely on such measurements to verify facility declarations. To aid in this objective, Los Alamos National Laboratory (LANL) developed the Portable Neutron Coincidence Counter (PNCC). This detector system was characterized using both the Neutron Coincidence Point Model and the new advanced multiplicity capability embedded in the Monte Carlo N-Particle extended (MCNPX) code. Characterization of this detector led to the creation of a reference model that can be used to immediately quantify the amount of plutonium (Pu) in a bulk sample based on its coincidence signature. Also, as a result of this characterization, the notion of using MCNPX and its new multiplicity capabilities as a tool for neutron coincidence counting analysis was studied in depth.

This thesis follows the style of *Nuclear Science and Engineering*.

THEORETICAL BACKGROUND

The most straightforward type of neutron counting is the measurement of totals rates. Each neutron that is detected produces one count, which contributes to the totals counts. This count is independent of time or location. Although easy to measure, the totals rates do not supply much information regarding the nuclear material measured. Coincidence counting, although a more difficult measurement technique, supplies far more useful information regarding the measured sample.

Neutron coincidence counting is a commonly used passive NDA technique used for quantitative and qualitative analysis of nuclear materials in bulk samples. NDA is the term applied to a wide range of nuclear material measurement techniques where the physical or chemical state of the material is not altered or destroyed. Passive NDA refers to the techniques that measure radiation emitted spontaneously from the nuclear material. This is method is often applied to Pu samples, because of the large spontaneous fission rate of the even Pu isotopes. Active NDA, on the other hand, refers to the techniques that measure induced radiation responses, often using an external neutron source, from a sample. These active methods are often applied to uranium measurements where the spontaneous fission rate is low.

During the fission process, multiple neutrons are simultaneously emitted from the fissioning nucleus. When two neutrons are emitted simultaneously, we refer to these neutrons as coincidence neutrons. To measure these coincident neutrons, time restraints must be applied to the detector. The gate-width is defined as a window of time within which the detection of more than one event can be linked. In other words, if two neutrons are detected within the pre-defined gate width, they can be assumed to have come from the same principle event.

Because coincidence neutron characteristics are specific to each isotope, the coincidence neutron signature can be used to characterize the nuclear material in the sample.

Plutonium specifically has a strong coincidence neutron signature due to the large spontaneous fission yields of the even atomic mass number isotopes (for example, ^{238}Pu, ^{240}Pu, and ^{242}Pu).

Although for plutonium, ^{238}Pu, ^{240}Pu, and ^{242}Pu all have dominant spontaneous fission yields; ^{240}Pu is of special interest because it is typically the major even isotope present in both low and high burn-up reactor grade Pu. It is therefore beneficial to relate the total amount of Pu in a sample to the amount of ^{240}Pu in a sample. This is accomplished by defining the ^{240}Pu effective mass. $^{240}Pu_{eff}$ is the mass of ^{240}Pu that would give the same coincidence response as that obtained from all the even isotopes in the actual sample. The ^{240}Pu effective mass can be determined using:

$$^{240}Pu_{eff} = 2.52\ ^{238}Pu + {}^{240}Pu + 1.68\ ^{242}Pu\ , \qquad \textit{(Eq. 1.1)}$$

where ^{238}Pu and ^{242}Pu are the masses of the corresponding isotopes[1]. The coefficients in Eq. 1.1 are constant and are primarily determined by the relative spontaneous fission half-lives and neutron multiplicity distributions of each isotope. Although the coincidence circuitry, or electronics package, could affect these coefficients, the impact is small because the spontaneous fission yields are the dominant effect. Therefore, the coefficients are essentially just the ratio of the spontaneous fission probability times the neutron multiplicity of each isotope to that of ^{240}Pu. These values are listed in Table 1.1.

Table 1.1. Spontaneous Fission Probabilities and Neutron Multiplicities for Various Pu Isotopes[1].

Isotope	Spontaneous Fission Yield (n/s-g)	Spontaneous Fission Multiplicity
^{238}Pu	2.59E+3	2.21
^{239}Pu	2.18E-2	2.16
^{240}Pu	1.02E+3	2.16
^{241}Pu	5.00E-2	2.25
^{242}Pu	1.72E+3	2.15
^{241}Am	1.18	3.22

From the amount of $^{240}Pu_{eff}$ in a sample, the total mass of Pu can be determined using:

$$Pu_{Total} = \frac{^{240}Pu_{eff}}{(2.52 f_{238} + f_{240} + 1.68 f_{242})}, \qquad \textit{(Eq. 1.2)}$$

where f_{238}, f_{240}, and f_{242} are the weight fractions of the plutonium isotopes, relative to the total Pu, present in the sample[1].

For PuO_2, which is the material used in this research, there are two principle sources of neutrons: spontaneous fission and (α,n) reactions. Several Pu isotopes decay by alpha emission. These alphas tend to undergo reactions with oxygen (O) in the sample producing singles neutrons[2]. Hence, coincidence counting measurements can be performed regardless of background or (α,n) neutrons present in the surrounding environment, because these neutrons occur in singlets. In other words, these neutrons are not emitted simultaneously with another neutron. This is convenient for measurements in various facilities because there are often other sources of radiation present in the background.

The difficulty involved with coincidence counting results from induced fission in the sample. Induced fission, also known as sample self-multiplication, occurs when neutrons in the sample, typically from (α,n) reactions or spontaneous fissions, cause a fission reaction and thereby increase the coincident neutron source. This source of error can be significant if not carefully considered.

With coincidence counting there are two observable parameters: the singles (or totals) rate and the doubles (or coincidence) rate. However, there are three unknowns: the mass of Pu in the sample, the (α,n) rate, and the neutron multiplication in the sample. In order to solve this dilemma, an assumed value must be used for either the (α,n) rate or the sample self-multiplication. Large errors may be introduced if this technique is not applied properly. It is common to use a Monte Carlo code to better determine these unknown parameters[3].

COINCIDENCE COUNTING INSTRUMENTATION

Thermal neutrons are generally easier to detect than fast neutrons. ^{3}He tubes, BF_3 tubes, and fission chambers are the traditional thermal neutron detectors. All take advantage of neutron interactions where charged particles are produced. These charged particles ionize the gas inside each detector producing a current. The most common type of detector used for neutron counting is the ^{3}He tube. These gas-filled detectors generally have high efficiencies and good reliability, are fairly rugged, and are, for the most part, insensitive to gamma radiation.

^{3}He tubes work by taking advantage of neutron interactions with ^{3}He atoms. The most probable reaction with ^{3}He is the (n,p) reaction which produces a proton and a triton (^{3}H). These resultant particles then ionize the ^{3}He gas producing a current that is proportional to the rate at which neutrons strike the detector.

The ^{3}He (n,p) reaction cross-section is shown in Figure 1.1. As can be seen, the cross-section is much larger for thermal neutrons (~ 0.0253 eV) than for fast neutrons (~ 1 MeV). Fission neutrons are born fast. Thus, to maximize the efficiency of the ^{3}He tubes, the neutrons must be slowed (or moderated) to thermal energies. Neutron moderation is most often achieved via elastic scattering collisions with hydrogenous material. For this reason, ^{3}He tubes are often embedded in high-density polyethylene (C_6H_{12}).

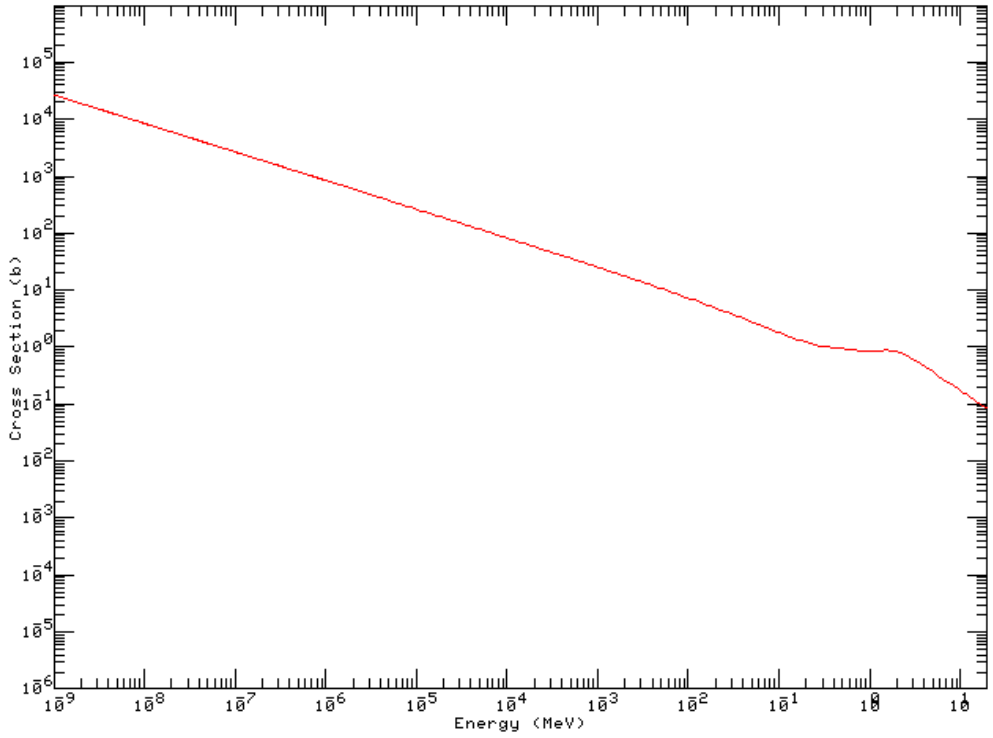

Figure 1.1. ^{3}He (n,p) cross-section as a function of neutron energy[4].

Neutron moderation significantly increases the time between neutron birth and its reaction in a detector. Because of this increased time, the gate width (predetermined time interval associated with a single event of the system) must be increased. This longer gate width can sometimes increase statistical error. It is typically assumed that for measured radiation, true events occurring in the detector follow a Poisson distribution. Dead-time losses, which increase with increasing gate width, essentially

remove counts from this distribution thereby distorting the Poisson distribution. Dead-time refers to the minimal amount of time required by the system to separate two events in order for them to be counted as two separate events[5].

Coincidence counting measurements are performed using sophisticated pulse processing electronics that measure the number of neutrons that are detected within a pre-defined time period (called a gate width). The gate width of the detector system should be very small, on the order of microseconds, so that if two neutrons are recorded in the small gate width, it can be assumed that they came from the same event, and therefore will be recorded as one doubles count.

The typical data collection system for neutron coincidence counting is a shift register whose main goal is to separate the incoming neutron pulse stream into correlated and uncorrelated events[6]. Correlated events refer to multiple radiation detections that stem from the same fission event, while uncorrelated events refer to detections that stem from different events. Typically, the detection of a neutron triggers the gate, which is open for a pre-defined time interval, or gate width. The next gate cannot begin until the first is complete. This leads to added dead-time in the detection process. The shift register, however, stores all incoming pulses for a time equivalent to that of the gate width. This decreases the number of detections lost due to detector dead-time and allows for the discrimination of correlated and uncorrelated neutrons.

One type of coincidence counter that is often used in safeguards measurements is the well counter. Well counters are large, bulky, require additional equipment for transport, and are usually accompanied by cumbersome electronics packages. Two customary well counters are shown in Figures 1.2 and 1.3. The High Level Neutron Coincidence Counter (HLNCC), shown in Figure 1.2, is an example of a passive NDA system, while the Active Well Coincidence Counter (AWCC), shown in Figure 1.3, is an example of an active NDA system[7]. Each well counter contains multiple ^{3}He tubes surrounded by a polyethylene matrix.

Figure 1.2. High Level Neutron Coincidence Counter.

Figure 1.3. Active Well Coincidence Counter.

These systems are very large (as implied by the wheels and dolly required to transport these systems) and restrict the location and environments in which measurements can be performed. The significant physical difference in the two detectors shown here is the presence of two americium-lithium (AmLi) sources in the AWCC; however, when used for Pu measurements these sources are removed and the system operates as a passive NDA system. For passive NDA measurements of Pu samples, the average detector efficiency is approximately 12 %. While 12 % efficiency is fairly high for neutron detectors, LANL developed the PNCC to eliminate the size, space, and location restrictions associated with the traditional well counters.

NEUTRON COINCIDENCE POINT MODEL

Neutron coincidence counting analysis is typically performed using the Neutron Coincidence Point Model[6]. The equations used in this model are derived using an actual sample in terms of the moments of the emitted and counted coincidence distribution. The singles and doubles rates, using the Neutron Coincidence Point Model, are given by:

$$S = m * F * \varepsilon * \nu_{s1} * M * (1+\alpha) \ , \qquad \textit{(Eq. 1.3)}$$

$$D = m * F * \frac{\varepsilon^2}{2} * f_d * M^2 * \left[\nu_{s2} + \frac{(M-1)}{(\nu_{i1}-1)} * \nu_{s1} * \nu_{i2} * (1+\alpha) \right] \ , \qquad \textit{(Eq. 1.4)}$$

where S is the singles count rate (in counts per second (cps)), D is the doubles count rate (in cps), m is the ^{240}Pu effective mass of the sample (in grams), F is the spontaneous fission rate (in f/s-g ^{240}Pu), ε is the detector efficiency (in counts per neutron), M is the leakage multiplication, α is the (α,n) to spontaneous fission neutron ratio, f_d is the doubles gate fraction, $\nu_{s1,}$ *and* ν_{s2} are the first and second reduced moments of the spontaneous fission neutron distribution, respectively, and $\nu_{i1,}$ *and* ν_{i2} are the first and second reduced moments of the induced fission neutron distribution, respectively.

The spontaneous fission rate (F) is defined as the number of spontaneous fissions per second emitted per gram of a particular isotope. For ^{240}Pu, the spontaneous fission rate is 473 f/s-g. The leakage multiplication (M) of a sample is a factor that represents the neutron multiplication in the sample due to other reactions, such as the (α,n) reaction with O. The leakage multiplication depends on the material and impurities in the sample. The reduced moments of the neutron distributions (ν_{s1}, ν_{s2}, ν_{i1}, and $\nu_{i,2}$,) are essentially the neutron multiplicities for spontaneous fission and induced fission. These values are constant for a particular isotope and are 2.154, 3.789, 3.163, and 8.24, respectively, for ^{240}Pu. The doubles gate fraction (f_d) is the ratio of the doubles efficiency for a finite gate width to that for an infinite gate width.

In most cases, m, F, ν_{s1}, ν_{s2}, ν_{i1}, and ν_{i2} are all known. These parameters are specific to the isotope of interest. M, ε, α, and f_d, however, are usually unknown and must be estimated (the efficiency can be measured). This is the most complicated part of neutron coincidence analysis. If these parameters are assumed incorrectly, the integrity of the results will be lost. Although the detector efficiency can be measured, there are still three unknowns and two equations. Therefore, the typical analytical processes involve

calculating one parameter (either α or M) using a Monte Carlo code (for example MCNPX).

There are a number of assumptions embedded in the point model. First, induced fission neutrons are assumed to be emitted simultaneously with the fission and/or (α,n) neutrons. Because particles emitted from fission occur within a very short time, this is a good assumption. If a neutron re-enters the sample and induces fission, however, this assumption breaks down.

Second, the model assumes that detector efficiency and probability of fission are uniform over the entire sample. For small homogeneous samples, this is a very good assumption. As the samples become larger, however, this assumption begins to break down. For plutonium oxide (PuO_2), this "point model" works well because the samples are diluted (with oxide) with respect to the neutron mean free path.

Third, the point model assumes that the spontaneous fission and (α,n) energy spectrum are consistent. This implies that F, ν_{s1}, ν_{s2}, ν_{i1}, ν_{i2}, and ε are the same for both neutron sources. This assumption is somewhat valid for PuO_2 samples because the neutrons from these sources have roughly the same average energy, just a different distribution. Using a detector that is energy independent is the best way to overcome error associated with this assumption.

Other assumptions include assuming it is valid to neglect neutron capture without fission, assuming neutron multiplicity and energy are not correlated, and assuming that neutron die-away time can be approximated by a single exponential time constant. These assumptions are appropriate for small detectors, such as the PNCC.

MCNPX CAPABILITIES

In the past, MCNPX has been used to generate either α or M. The process of creating a model to calculate particular parameters and using them in the point model equations is time-consuming and cumbersome. Fortunately, the newest versions of MCNPX have incorporated new multiplicity capabilities that allow detector responses to be directly simulated by the computational model using a new ^{3}He capture tally[8].

This feature is embedded inside the F8 tally. Using the FT8 card, the F8 tally is converted from a pulse height tally to a neutron coincidence capture tally. This tally scores the number of captures in the specified nuclide(s) (^{3}He in this case) at the end of each particle history.

For coincidence counting applications, it is useful to include a pre-delay, the time delay before the gate begins, and gate width on this card. Other optional parameters available in the capture tally include the maximum number of captures and the maximum number of moments. The default values of 21 and 12, respectively, were used for this research. When using the F8 tally, no variance reduction may be used. Calculations must be analog and fission multiplicity is required.

Because this new feature embedded in MCNPX allows the already needed computational model to simulate the detector response directly, it may eliminate the need for the Neutron Coincidence Point Model altogether.

OVERVIEW

Based on coincidence counting measurements performed on a series of known PuO_2 standards, an analysis was performed to thoroughly compare the results obtained using the Neutron Coincidence Point Model and the results from the direct detector simulation using MCNPX. This analysis will attempt to show that the multiplicity capabilities in

MCNPX make it a sufficient and viable tool for coincidence counting measurement and analysis.

The PNCC will be described in detail, and the initial characterization of the system will be analyzed and discussed in Chapter II. The PuO_2 measurements will be discussed in Chapter III. Chapter IV will cover the MCNPX modeling of the system and standards. The results will be given and discussed in length. The Neutron Coincidence Point Model results will be analyzed and discussed in Chapter V. These results will then be compared to the MCNPX results and the measured data to compare the two methods of analysis. A sensitivity analysis will be discussed in Chapter VI and the conclusions will be given in Chapter VII.

CHAPTER II

PORTABLE NEUTRON COINCIDENCE COUNTER

The PNCC was developed by LANL to aid the IAEA in the measurement of nuclear materials. The system consists of four individual slab detectors that can operate in multiple modes and configurations. The detector is lightweight and portable making it ideal for various laboratory and field environments.

The small size and portability of this detector system would give an inspector the freedom to adapt his/her measurements to the sample in question with little restriction regarding space or location, which can be a very limiting factor in some applications. This gives the inspectors flexibility they do not have when using the traditional well-type coincidence counters.

PHYSICAL DESCRIPTION

The PNCC consists of four high-density (0.25 g/cc) polyethylene slabs. Each slab has dimensions of 17.8 cm (length) x 22.9 cm (height) x 7.6 cm (width). Each slab weighs approximately 3.8 kg. Embedded in each polyethylene slab are four ^{3}He tubes. The 10 atm ^{3}He tubes are 2.54 cm in diameter and 25.4 cm long with an 18 cm active length. Each tube has aluminum walls of 0.762 mm thickness. The ^{3}He tubes extend the full length of the polyethylene slab and are interconnected through the junction box residing on the top of each slab. Figure 2.1 shows an individual slab including the four ^{3}He tubes, polyethylene moderator, and electronic junction box.

The aluminum junction box is 2.54 cm tall and houses the onboard electronics package for each detector. This electronics package includes the pre-amplifier, the amplifier, and the discriminator, and supports the high voltage and detector bias. The pre-amplifier is used to convert the charge in the detector to a voltage pulse and provide some signal

shaping and filtering. The amplifier provides the major amplification and shaping of the pulse. The discriminator measures the energy of the amplified pulse to determine whether it qualifies as an event and then converts the output pulse to a logic signal. This signal is then output to the counting equipment.

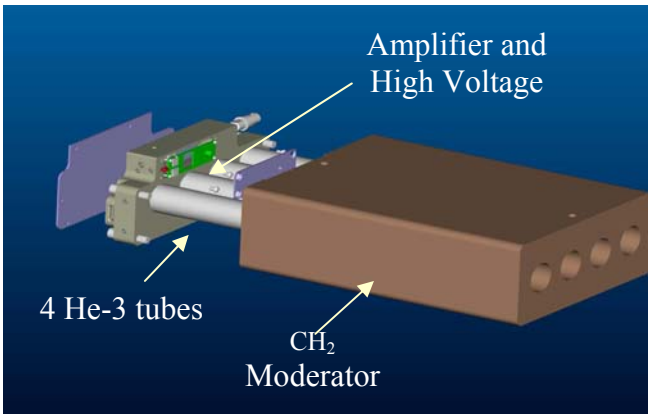

Figure 2.1. Individual Slab of PNCC.

One advantage of the PNCC is that it can be used in multiple configurations. The two configurations considered here are the four-slab model and the two-slab model. The four-slab model involves placing the four polyethylene slabs corner-to-corner in a collar-type arrangement, shown in Figure 2.2. Figure 2.3 shows the two-slab configuration, which involves two slabs that are coupled by two solid polyethylene brackets. These side brackets increase the efficiency of the system as well as help to ensure consistent geometry. This flexibility allows the user to better accommodate any particular sample of interest. The research and analysis discussed in this thesis is based on the four-slab configuration.

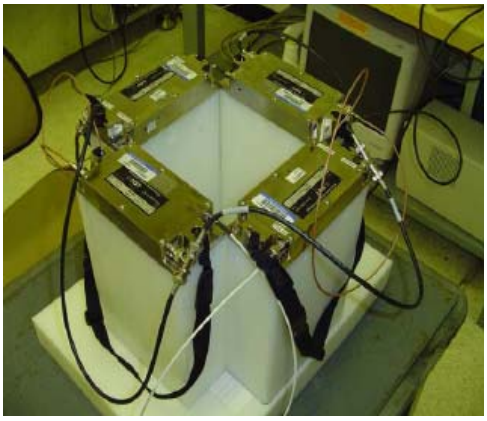

Figure 2.2. Four-slab configuration.

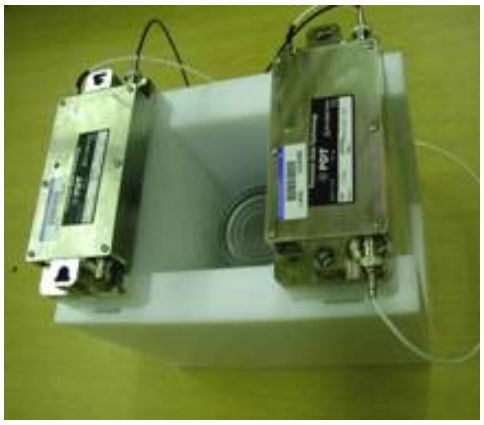

Figure 2.3. Two-slab configuration.

CHARACTERIZATION

Experiments were performed to provide a detailed characterization of the PNCC. The characteristics measured were the detector efficiency, high-voltage plateau, and symmetric behavior of the system. The detector efficiency refers to how well the detector detects the particle of interest and is defined as the number of radiation quanta detected divided by the total number of radiation quanta emitted by the sample. The high-voltage plateau indicates the voltage region in which the detector response is the most stable. The geometric behavior of the system is important for symmetry, replication, and optimization.

Each of these characteristics can be determined using various measurement techniques. All measurements were performed in an open laboratory with californium (^{252}Cf) sources. The PNCC was setup in the four-slab configuration on a 1" thick wooden table. The slab detectors were isolated from the wooden table using a 2" thick piece of polyethylene.

Detector Efficiency

To determine the detector efficiency, a small ^{252}Cf point source was placed in the center of the sample volume between the four slab detectors. This source had a calibrated source strength of 2.013E+5 n/s on October 1, 2002. Ninety 10-second measurements were recorded using the IAEA Neutron Coincidence Counting (INCC) software[9]. This software will be described in more detail in Chapter III. Table 2.1 lists the average count rates recorded as well as the neutron source strength of the ^{252}Cf source at the time of the measurements. This source strength was calculated based on the decay correction of the source strength reported on the source ID tag. The uncertainty was assumed to be less than 5 % based on the source origins. The detector efficiency (ε) was then determined using:

$$\varepsilon = \frac{S}{Y}, \qquad \textit{Eq. 2.1}$$

where S is the singles count rate (in cps) and Y is the source strength (in n/s).

The efficiency of the PNCC at the center of the sample volume based on the ^{252}Cf point source measurements was determined to be 8.9 ± 0.4 %. This is a fairly good efficiency considering the size of the detector system. Recall that traditional well counters typically have an efficiency of approximately 12 %, but are very large and inconvenient for portable use. Based on this result alone, the PNCC appears to be an adequately efficient coincidence counter.

Table 2.1. Detector Efficiency Data.

Date of Measurement	03/17/2005
Singles Count Rate (cps)	9373 ± 2
Doubles Count Rate (cps)	824 ± 1
Neutron Source Strength on Date of Measurement (n/s)	105219 ± 5261
Detector Efficiency (%)	8.9 ± 0.4

Voltage Plateau

The high-voltage plateau was determined through a series of measurements with the detector operating at different voltages. The same ^{252}Cf point source (as was used in the efficiency measurements) was placed in the center of the sample volume. Beginning with the high-voltage set at 1500 V, the totals count rates for ninety 10-second measurements were recorded. The high-voltage was then increased by 20 V, and the measurement was repeated. This continued until a high voltage of 1800 V was reached.

The totals count rate was then plotted as a function of high-voltage. This curve is shown in Figure 2.4 and is typically known as a high-voltage curve. The error bars are included but are too small to be visible. Ideally, the detector should operate on the flattest region (or plateau) of this curve so that slight changes (or drifts) in high voltage will not affect the count rates in the system. 1680 V was determined to be the optimal operating high-voltage because of its location on the flattest part of the curve.

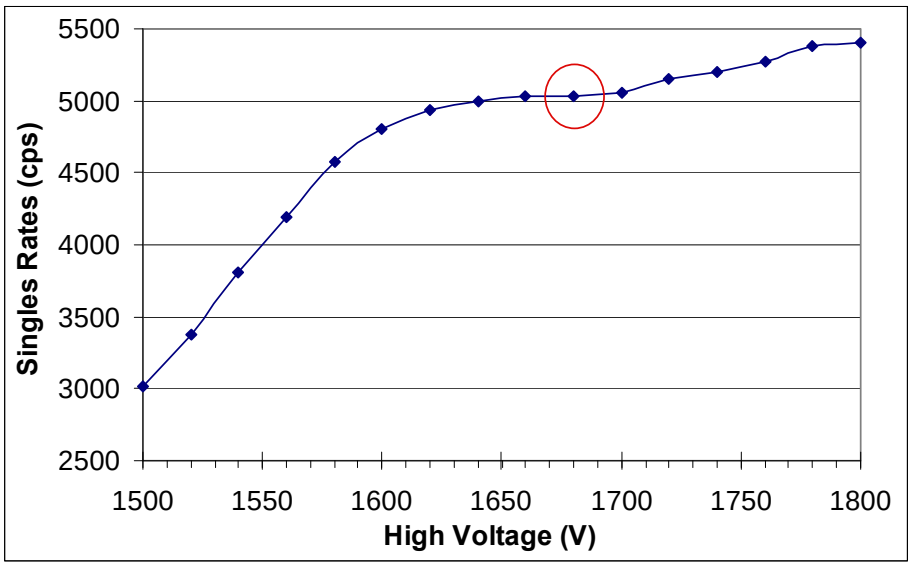

Figure 2.4. High voltage plateau.

Vertical and Horizontal Profiles

The symmetric behavior of the detector system was determined using vertical and horizontal profiles. These profiles were obtained by measuring the same ^{252}Cf source (as was used above) at designated locations inside the sample area. These locations were chosen at various incremental horizontal and vertical positions. Ninety 10-second measurements were recorded for each source location. The average of these ninety measurements was used to calculate detector efficiency for each position. These efficiencies were then plotted as a function of the x, y, and z position of the source to create the horizontal and vertical profiles shown in Figures 2.5 and 2.6. The error bars are present in the figures, but again are too small to observe.

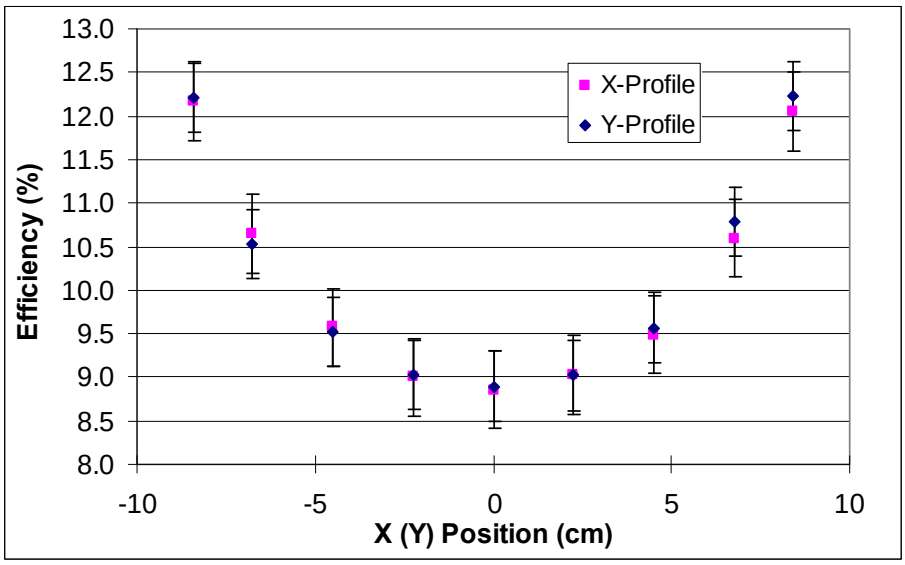

Figure 2.5. Horizontal efficiency profiles.

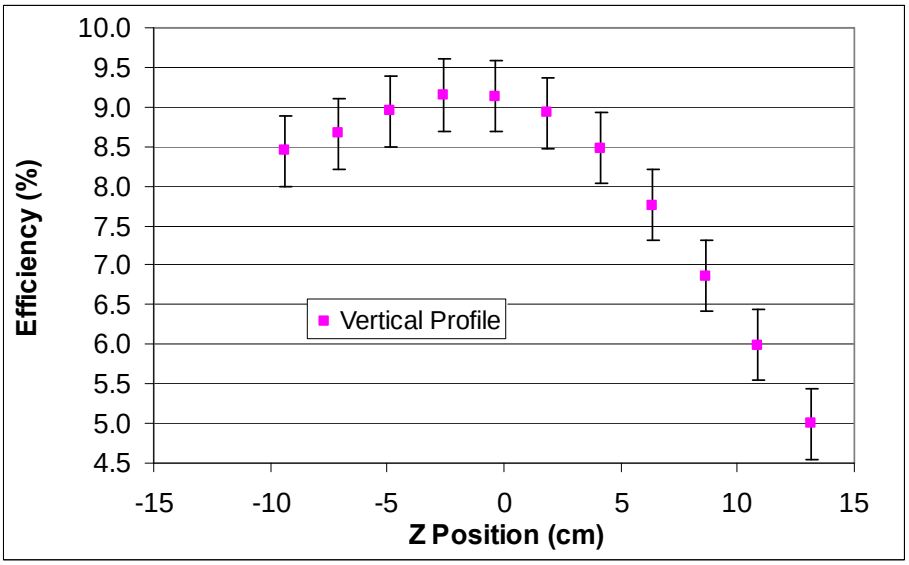

Figure 2.6. Vertical efficiency profile.

As was expected, Figure 2.5 and 2.6 show that the system is symmetric in the x- and y-directions. This implies that each detector slab contributes equally to the overall system and can be interchanged without affecting the outcome of the measurements. This symmetry helps ensure that the measurements can be repeated regardless of the specific slab being used. It is also important to note that the efficiency reported above is the system efficiency for a neutron born at the center of the configuration. Based on these figures, the efficiency away from the center toward any side in the x- or y- direction would actually be higher.

The vertical profile shows that the maximum efficiency occurs with material slightly below the vertical center. This is primarily caused by the reflection of neutrons from the polyethylene slab under the detectors and the leakage of neutrons out of the top of the system. This effect could be reduced by placing a polyethylene slab on top of the four-slab system.

Assessment of Characterization of PNCC

After the initial characterization of the PNCC, it was determined that the system works properly. The reasonably high efficiency of the system shows that the quality of the system has not been compromised by its small size, and that it can be used for practical coincidence counting measurements. The optimum operating high voltage is easily achievable and ensures consistent detector response. The symmetry of the system shows that the individual slab detectors are matched well and contribute evenly. These characteristics are vital in ensuring the integrity of the measurements.

APPLICATIONS

Once characterized, the PNCC can be operated in several different modes. Each detector slab can operate alone or combined with each other in chain. When the detectors are chained, the output is sent to a shift register. The shift register provides the external voltage for the detectors and acts as the data collection system. The detectors can be

used to measure single counts, ideal for large area surveys where direction sensitivity is desired, or in coincidence mode, which takes advantage of isotope signatures based on coincident neutrons[10].

The primary applications for the PNCC will be to assist nuclear inspectors from the IAEA to verify nuclear materials in various laboratory and field environments. The goal is to be able to carry the detector system inside a carry-on size suitcase into any facility to perform both survey measurements and coincidence measurements on various samples.

LIMITATIONS

While the portability of the PNCC makes it a desirable instrument for neutron coincidence counting measurements, it has some drawbacks. Limitations of the PNCC involve the sample material, size, and content, and other existing environmental conditions. The fundamental limitation with any passive NDA system is that it is nearly impossible to measure U samples, or other materials that are heavily shielded. These types of measurements are typically done using neutron interrogation methods such as active NDA.

In the four-slab configuration discussed earlier, the system can accommodate a maximum sample diameter of 17 cm. The two-slab configuration can only accommodate a diameter of 11 cm. A sample with a larger diameter would change the geometry of the problem, and the PNCC would need to be re-characterized for this configuration.

The sample content is another important limitation. As will be discussed in more detail later, the density and water content of the sample will most likely be unknown at the time of the measurement. The density affects the height of the nuclear material in the sample and therefore changes the geometry of the measurement. Water content

effectively changes the density of the sample and adds to the uncertainty of the problem. The extent of these problems will be discussed further in later chapters.

Environmental factors play an important role in the uncertainty of the measurements. If there are strong neutron sources nearby, they could induce more fissions and lead to false coincident events. Other nearby materials, such as strong reflectors, can also contribute to the error in detector response. To reduce this problem, care should be taken when setting up the measurements.

CHAPTER III

PLUTONIUM MEASUREMENTS

As an inspector measuring unknown nuclear samples, it would be useful to have some reference model for the PNCC that would enable you to immediately quantify the amount of Pu in a bulk sample based on the coincidence signatures measured. Such a reference model was created using a series of known Pu standards. This would allow an inspector to simply look at a graph or table, and estimate the amount of Pu present based on the doubles count rate measured using the PNCC.

PLUTONIUM STANDARDS

In order to create a reference model for the PNCC, it was necessary to perform a number of measurements using various known Pu standards. Four PuO_2 samples with known isotopics were used. These standards, known as the Los Alamos Operations (LAO) PuO_2 powder series are described in Table 3.1. Note that the ^{241}Am is not included in the Pu mass nor was it used to calculate the $^{240}Pu_{eff}$ mass. The calculated ^{240}Pu effective mass (see Eq. 1.1) for each standard is also given in the table.

Table 3.1. Pu Mass and Isotopics for PuO_2 Standards.

Sample ID	Pu Mass (g)	^{238}Pu (w/o)	^{239}Pu (w/o)	^{240}Pu (w/o)	^{241}Pu (w/o)	^{242}Pu (w/o)	^{241}Am (w/o)	$^{240}Pu_{eff}$ (g)
LAO-251	172	0.06	82.66	16.47	0.47	0.35	0.96	29.6
LAO-252	322	0.05	82.81	16.33	0.46	0.35	0.93	54.9
LAO-255	544	0.06	82.77	16.37	0.46	0.34	0.93	93.0
LAO-256	385	0.05	82.79	16.36	0.45	0.34	0.91	65.7

The Pu mass given here is the total mass of Pu in each sample. The weight percent of each isotope is also shown here. It should be noted that the weight percents of each isotope in the sample are consistent for all four samples. In other words, the ratio of each isotope, ^{238}Pu for example, to total Pu is roughly the same for each standard. Note that the difference in total Pu mass between the smallest and largest sample is 372 grams. The $^{240}Pu_{eff}$ mass also ranges significantly from the smallest to largest sample.

Although given the Pu mass and isotopics, it must be understood that the Pu in these samples is in the form of PuO_2 powder. As previously mentioned, the O in the sample plays an important role in coincidence counting measurements. Most of Pu isotopes decay by alpha emission, some of which undergo an (α,n) reaction with O in the sample. These reactions produce additional singles neutrons in the sample. These neutrons are then free to induce fission in other Pu isotopes, causing more coincidence neutrons than would be present if the sample consisted of only Pu metal. Therefore, it is important to take the oxide in the PuO_2 samples into account. Table 3.2 shows the total sample mass and weight percent of each isotope, including the oxide. Note that no uncertainties were reported with the isotopics, however, they are assumed very accurate since the PuO_2 samples are standards.

Table 3.2. Total Mass and Isotopics for PuO_2 Standards.

Sample ID	**PuO_2 Mass (g)**	**^{238}Pu (w/o)**	**^{239}Pu (w/o)**	**^{240}Pu (w/o)**	**^{241}Pu (w/o)**	**^{242}Pu (w/o)**	**^{241}Am (w/o)**	**^{16}O (w/o)**
LAO-251	195	0.05	72.91	14.52	0.41	0.31	0.85	11.80
LAO-252	365	0.05	73.04	14.41	0.40	0.31	0.82	11.80
LAO-255	617	0.05	73.00	14.44	0.40	0.30	0.82	11.80
LAO-256	436	0.05	73.02	14.43	0.40	0.30	0.80	11.80

Another important characteristic taken into consideration was the density of the sample. Because the samples contain PuO_2 powder, the densities were unknown. If the sample had been sitting for months, the powder would settle toward the bottom of the sample container increasing the density. If the sample had been shaken or turned upside down, the density of the powder might be less.

The density affects the sample in that it changes the self-multiplication and self-absorption in the sample. For example, an increase in density would provide more neutron absorption and neutron multiplication; however, it would also decrease the volume of the sample for a given total Pu mass. Since the detector efficiency is sensitive to the sample position this volume distribution is important (see Figures 2.5 and 2.6). The effect on the count rates would depend on the combination of these competing effects.

Although the densities of the material in each standard were unknown, they were estimated to be approximately 0.9 g/cc. This estimate was based on the origins of the PuO_2 in the samples. The standards were fabricated from very pure oxide leftover from the production of fuel feed for the Fast Flux Test Facility (FFTF) in Richland, Washington. The fuel feed for the FFTF was composed of mixed-oxide (MOX) fuel of very pure PuO_2 and UO_2. The density range of this MOX fuel for the purposes of use in the FFTF was 0.7- 1.2 g/cc. Therefore, it was assumed that the leftover powder would have a density within this range. A density of 0.9 g/cc was chosen because it is in the center of this range. The effects of assuming this density will be address in later sections.

Each of the four PuO_2 standards was in a container that used the same canning materials and had the same dimensions. Each sample was double canned, as is standard for Pu samples, using stainless steel. The outer diameter of each sample was measured to be 13.335 cm, while the inner canning was estimated to be inset by about 1.3 cm on each side. The height of the outer canister was measured to be 15.24 cm. The bottom of the inner canning was estimated to be elevated approximately 0.76 cm inside the outer

canning. It is important to note that the inner dimensions of the canning were assumed. Table 3.3 gives the geometric dimensions of the samples and includes the fill height of the each standard.

Table 3.3. Geometric Properties of PuO_2 Standards.

Sample ID	Mass (g)	Sample Density (g/cc)	Inner Volume (cc)	Inner Radius (cm)	Inner Height (cm)	Fill Height (cm)
LAO-251	195	0.9	216.7	5.4356	12.7	2.33
LAO-252	365	0.9	405.6	5.4356	12.7	4.37
LAO-255	617	0.9	685.3	5.4356	12.7	7.38
LAO-256	436	0.9	485.0	5.4356	12.7	5.23

The fill height is of great importance because it has the potential to change the geometry of the measurements. As shown earlier, the efficiency of the system as a function of vertical location is not constant (see Figure 2.6). The efficiency of the top of the system is lower than that towards the bottom of the system. For optimal efficiency, the nuclear material should be placed accordingly; however, because the inner dimensions are not known, the exact location of the nuclear material inside is not known. Therefore, this may be a potential source of error.

MEASUREMENTS

The measurements made using the PuO_2 standards described above were performed using the PNCC in the four-slab configuration, shown in Figure 2.2. The detectors were connected as illustrated in Figure 3.1. The shift register used for these measurements was a JSR-11 Shift Register. This shift register output the +5 V required for detector operation to the first slab detector in the chain. The low voltage was transferred to each

consecutive slab via coaxial cables, represented in blue. The detector signal cables, in red, summed the individual detector responses and sent them back into the shift register for processing. Once processed by the shift register, the acquisition computer collected the data. INCC software was then used to analyze the data.

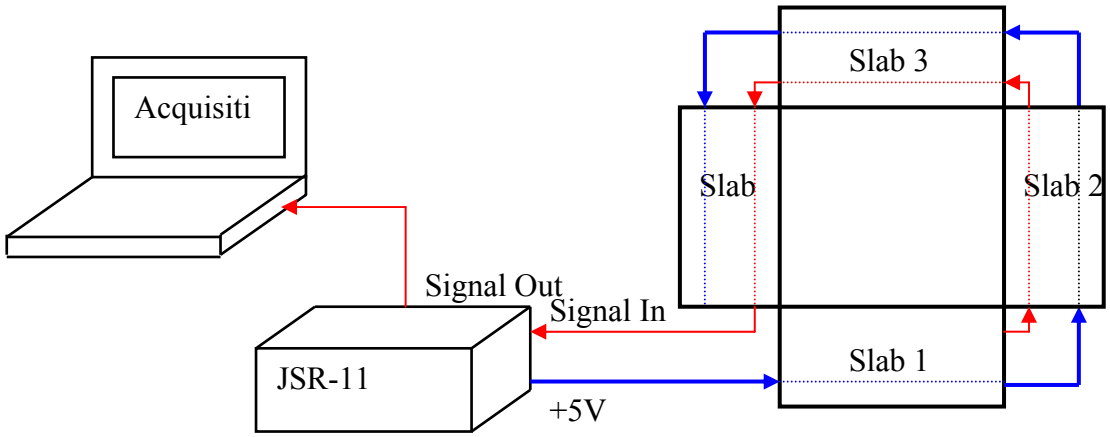

Figure 3.1. Low voltage and signal flow schematic.

INCC was developed by ORTEC to aid the IAEA in neutron coincident counting measurements. The software acts as a hardware interface, allowing the user to change or set detection parameters in the shift register, most importantly the gate width and measurement times. The software allows for analysis in *Rates Only* mode where singles, doubles, and triples count rates along with errors are reported. These values are corrected for detector dead-time, passive background, and normalizations. Although the optimal gate width was determined to be approximately 40 μs, a gate width of 64 μs was assigned using the INCC software. This gate width was used because it is the default gate-width. A pre-delay was set to 4.5 μs, and the number of cycles and length of each cycle was set for ninety counts, 10 seconds each.

These measurements were performed in a large open laboratory on a 1" thick wooden table. The PNCC was isolated from the table and the cement floor by placing a 2" thick polyethylene slab beneath the detector configuration. While shielding was in place to isolate the measurements from contamination, there were large Pu sources moving in and around the laboratory. All attempts were made to perform counts only when the other Pu sources were not exposed in the room. A paper grid, marked in centimeter increments, was placed at the bottom of the sample area to sustain consistency in the placement of the PuO_2 standards.

First, a background measurement was performed. Without a sample present, ninety 10-second counts were recorded. This background rate was then stored and automatically incorporated so that net count rates are given by the analysis performed using INCC. The average count rates reported have all been corrected for dead-time and background rates.

The first PuO_2 standard was then placed on top of the grid at the center of the sample area. The data acquisition software was started using the INCC software. After ninety 10-second counts were completed, the data was saved. The sample was removed and stored away from the detector. The next sample was placed in the sample area. Again, ninety, 10-second counts were measured, and the data was stored. This method was repeated for the remained two PuO_2 standards.

RESULTS AND ANALYSIS

The singles and doubles rates, all given in cps, and the corresponding errors were all recorded with INCC. These data are shown in Table 3.4. The background count rate was reportedly 145 ± 2 cps; however, this was already taken into account by the software and is incorporated in the results shown in Table 3.4. As expected, the trends show that the larger samples have higher singles and doubles rates. The errors reported are all 1-σ standard deviations.

Table 3.4. Measured PuO_2 Data. (dead-time and background corrected)

Sample ID	Singles Count Rate (cps)	Doubles Count Rate (cps)
LAO-251	3721 ± 5	132 ± 2
LAO-252	7017 ± 3	268 ± 2
LAO-255	12191 ± 4	493 ± 4
LAO-256	8369 ± 4	329 ± 3

The spontaneous fission neutron source strength (Y_{SF}) for each sample was calculated using:

$$Y_{SF}\left(\frac{n}{s}\right) = 1020\left\{2.43\left[\frac{f_{238} * m_{total}}{100}\right] + \left[\frac{f_{240} * m_{total}}{100}\right] + 1.68\left[\frac{f_{242} * m_{total}}{100}\right]\right\}, \quad \textit{(Eq. 3.1)}$$

where f_{238}, f_{240}, and f_{242} represent the weight percent of the corresponding isotope relative to the total amount of Pu in the sample, m_{total} is the total sample mass (in g), and the coefficients are based on the spontaneous fission neutron yields (n/s-g) for the various Pu isotopes. The coefficients are based on the spontaneous fission neutron yields (n/s-g) for the specified Pu isotopes (see Table 1.1). The (α,n) neutron source strength ($Y_{(\alpha,n)}$) for each sample was calculated using:

$$Y_{(\alpha,n)}\left(\frac{n}{s}\right) = 13400\left[\frac{f_{238} * m_{total}}{100}\right] + 38.1\left[\frac{f_{239} * m_{total}}{100}\right] + 141\left[\frac{f_{240} * m_{total}}{100}\right]$$

$$+1.3\left[\frac{f_{241} * m_{total}}{100}\right] + 2\left[\frac{f_{242} * m_{total}}{100}\right] + 2690\left[\frac{f_{Am-241} * m_{total}}{100}\right], \quad \textit{(Eq. 3.2)}$$

where, f_{238}, f_{239}, f_{240}, f_{241}, f_{242}, *and* f_{Am241} represent the weight percent of the corresponding isotope relative to the total amount of Pu in the sample, m_{total} is the total sample mass (in g), and the coefficients are based on the (α,n) neutron yields in oxide (n/s-g) for the various Pu isotopes. These coefficient are simply the (α,n) yield in oxide for the respective isotopes, given in Table 3.5.

Table 3.5. (α,n) Yield in Oxide for Pu Isotopes[1].

Isotope	**(α, n) Yield in Oxide (n/s-g)**
^{238}Pu	1.34E+4
^{239}Pu	3.81E+1
^{240}Pu	1.41E+2
^{241}Pu	1.3
^{242}Pu	2.0
^{241}Am	2.69E+3

The detector efficiency (ε) was then calculated using:

$$\varepsilon = \frac{S}{Y_{SF} + Y_{(\alpha,n)}} \quad , \qquad \textit{(Eq. 3.3)}$$

where S is the singles count rate and Y_{SF} and $Y_{(\alpha,n)}$ are given in Equations 3.1 and 3.2, respectively.

The detector efficiencies, spontaneous fission neutron yields, and (α,n) neutron yields for each of the four PuO_2 samples can be found in Table 3.6. Again, as expected, the larger samples yield more neutrons and have higher efficiencies. The uncertainties reported are very small since there were no reported uncertainties listed with the

isotopics. It is important to note that on average the efficiencies listed here fall within the error bars of the point source measurement (see Table 2.1).

Table 3.6. Measured Efficiencies and Neutron Yields.

Sample ID	Mass (g)	SF Yield [n/s]	(α,n) [n/s]	Efficiency (%)
LAO-251	195	30150	15130	8.2178 ± 0.0001
LAO-252	365	55946	27769	8.38201 ± 0.00004
LAO-255	617	94855	47672	8.55335 ± 0.00003
LAO-256	436	66999	33118	8.35922 ± 0.00004

Because it is the coincidence signature that leads to the quantification of Pu in bulk samples, the measured doubles rates were plotted as a function of $^{240}Pu_{eff}$ mass. This graph, referred to as the reference model for the PNCC, is shown in Figure 3.2. Note that error bars are included on the plot but are generally too small to be visible. Interpolated values from this plot are listed in Table 3.7.

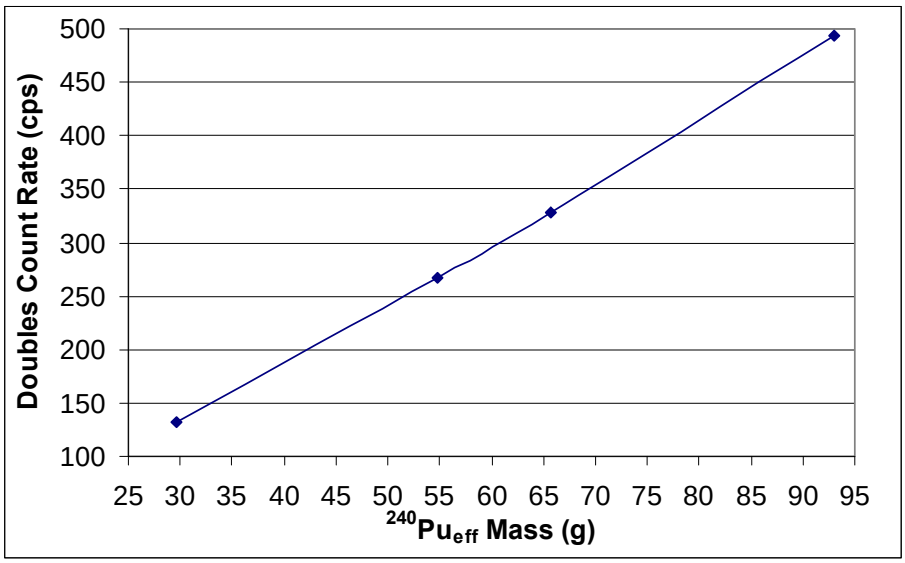

Figure 3.2. Measured doubles rates as a function of $^{240}Pu_{eff}$ mass.

Table 3.7. Tabulated Values for Reference Model.

Coincidence Count Rate (cps)	**$^{240}Pu_{eff}$ Mass (g)**	**Coincidence Count Rate (cps)**	**$^{240}Pu_{eff}$ Mass (g)**
102	25	**329**	65
130	30	**358**	70
159	35	**386**	75
187	40	**415**	80
216	45	**443**	85
244	50	**472**	90
273	55	**500**	95
301	60	**-**	-

DISCUSSION

The PNCC measurements provided singles and doubles count rates for four PuO_2 standards ranging in mass from 195 g to 617 g. As expected, the data shows that the more Pu present in a sample, the higher the singles and doubles count rates. These increasing trends are linear; therefore, linear interpolation was used to tabulate the values in Table 3.7.

The calculated efficiencies, based on the measured data, ranged from 8.2 % to 8.6 %. As expected, this is slightly lower than the system efficiency of 8.9 % reported in Table 2.1. This is primarily due to the larger size of the PuO_2 samples; the system efficiency was originally determined using a ^{252}Cf point source. This range of efficiencies also gives a range of interest for varying Pu samples. An efficiency of more that 8 % is acceptable, considering the size and flexibility of the PNCC. This shows that the PNCC is useful detection system for neutron coincidence counting applications.

These coincidence measurements also provided the necessary doubles count rates to create a PNCC reference model. Ideally, an inspector in the field would perform similar neutron coincidence measurements. Immediately after the data is collected, the inspector could refer to the reference model (plot or table) and estimate the amount of $^{240}Pu_{eff}$ in the sample. For example, if the results of the coincidence measurement reported a doubles count rate of 200 cps, the inspector could use the table and estimate that between 40 and 45 grams of Pu are in the sample. This reference model allows for simple and immediate verification of material declarations.

To test agreement with the reference model, more known standards should be measured. The doubles rates and Pu mass should then be verified using the model. As will be discussed later, the reference model will also be analyzed in comparison to the Neutron Coincidence Point Model and MCNPX. This analysis will help qualify the reference model for use in other neutron coincidence counting applications.

There are a number of sources that can potentially generate error in measured data. Statistical error due to counting equipment and human error are two common sources. For this specific set of measurements, there was additional error in that there were multiple neutron sources moving in and around the measurement area. While this may be bothersome in other cases, it is something that may very well be unavoidable in applications where the PNCC will be deployed.

CHAPTER IV

COMPUTATIONAL MODEL

The most common analysis technique used for neutron coincidence counting is the Neutron Coincidence Point Model. However, as previously discussed, the point model for coincidence counting involves two equations and three unknowns. To estimate the third unknown, a Monte Carlo simulation is often performed. Typically, MCNP is used to generate either the (α,n) rate (α) or the neutron multiplication (M). These values, once calculated, are extracted from the MCNP output and used in the point model equations (see Eqs. 1.3 and 1.4).

MCNPX, however, has incorporated a new advanced multiplicity capability that directly simulates detector response. This new capability is embedded in an F8 capture tally, which takes advantage of neutron capture in ^{3}He. Because of this direct simulation, it may be possible to use MCNPX alone to perform neutron coincidence counting analyses eliminating the need for the Neutron Coincidence Point Model.

PORTABLE NEUTRON COINCIDENCE COUNTER MODELING

The computational model of the PNCC was based on the physical description discussed in Chapter II. Each high-density, 0.25 g/cc, polyethylene slab was modeled as a 17.8 cm x 22.9 cm x 7.6 cm slab with four 2.8575 cm diameter cylinders bored out the entire length of the slab. Centered in each of these empty cylinders were the ^{3}He tubes. The inner diameter of the ^{3}He tubes was 2.386 cm. The active regions, the middle 17.8 cm of the ^{3}He tubes were filled with ^{3}He gas with a density of 2.4463e-4 atoms/(b-cm). The inactive regions on both top and bottom were filled with air. The aluminum cladding was 0.76 mm thick and had a density of 2.7 g/cc. The gap between the aluminum cladding and the polyethylene was filled with air at a density of 0.001293 g/cc.

The junction box, which houses the onboard electronics, was modeled as a 2.54 cm iron box with density 2.0 g/cc. Although the junction box is not a solid Fe box, its presence was not expected to affect the results substantially because it is located at the top of the system where neutron leakage is high. Note also that it is located above the inactive regions of the ^{3}He tubes.

The four-slab configuration was modeled sitting atop a solid 5.08 cm high-density polyethylene slab. A 3-D picture of the MCNPX model is shown in Figure 4.1. The picture was generated using SABRINA[11], a graphics code used to create 3-D plots of MCNP geometries. The grey material represents the polyethylene while the maroon represents the iron junction boxes. The ^{3}He tubes, inside the polyethylene slabs, are represented in green.

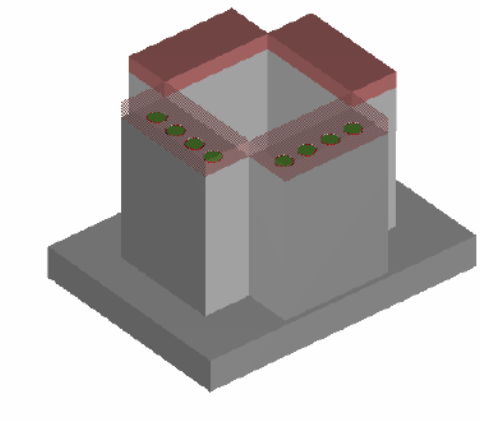

Figure 4.1. 3-D MCNPX model of PNCC

Figure 4.2 shows a 2-D top-view of the four-slab configuration generated using MCNP-VISED 4C2[12], a tool that provides visual 2-D geometry, based on the MCNP input. The ^{3}He tubes are easily identifiable. The ^{3}He gas is represented in yellow. The green region outlining the ^{3}He gas is the aluminum cladding. The red signifies the

polyethylene slabs surrounding the ^{3}He tubes. The pink color represents the sample volume between the four slab detectors.

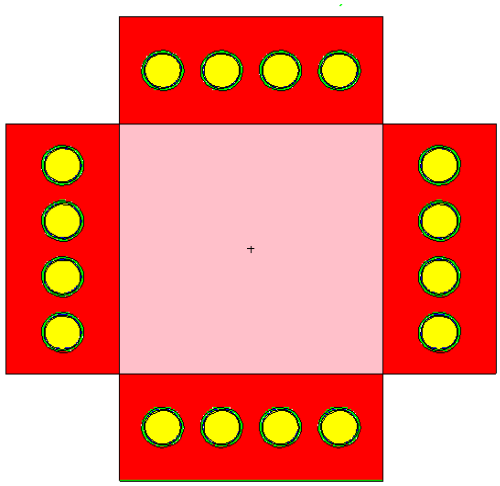

Figure 4.2. 2-D MCNPX model top view of PNCC.

PLUTONIUM SAMPLE MODELING

In order to generate parameters that are usable in the Neutron Coincidence Point Model analysis, the samples modeled in MCNPX must be the same as the samples that were measured. This includes the physical characteristics and the material composition. The difficulty in modeling these PuO_2 samples was that a few of the sample characteristics were not fully known.

The density is one example of an unknown characteristic. Again, because the material is a powder, the density can change based on settling. The density is important in that it defines the fill height for each sample. Because the samples are large relative to the detector, the height of the sample may influence the efficiency of the system. As discussed in Chapter III, the density also affects the neutron multiplication and absorption, which are competing effects that could affect the calculated results. Recall

from Chapter III that 0.9 g/cc was chosen as the sample density and was used for all of the calculations performed here.

Another unknown parameter in these calculations is the inner canning of the PuO_2 standards. Because the inner can dimensions were not known, approximations were used. These dimensions could be important because they affect the fill height and location of the Pu in the sample. Again, these effects can change the count rates because as shown in Figures 2.5 and 2.6, the efficiency of the PNCC is dependent upon the location of the material inside the detection system. The diameter of the inner canning was estimated to be 10.87 cm and was assumed to be elevated by 0.764 cm. Figure 4.3 shows the assumed dimensions of the PuO_2 canister. The hatched region represents the nuclear material.

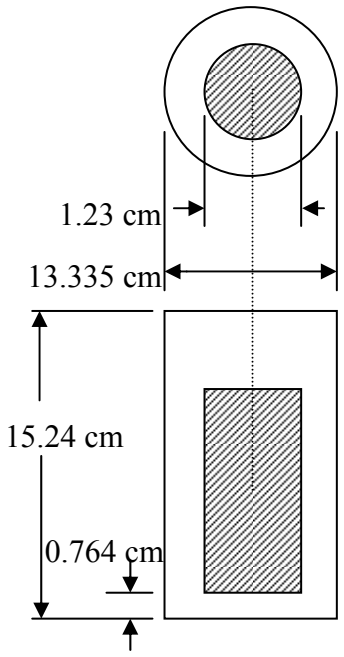

Figure 4.3. PuO_2 canister schematic.

The fill height of the nuclear material varied for each sample size. Table 4.1 lists the total sample masses and corresponding fill heights. The assumed densities and inner canning radii are also given.

Table 4.1. MCNPX Sample Geometry Parameters.

Sample ID	Mass (g)	Sample Density (g/cc)	Inner Radius (cm)	Fill Height (cm)
LAO-251	195	0.9	5.4356	2.33
LAO-252	365	0.9	5.4356	4.37
LAO-255	617	0.9	5.4356	7.38
LAO-256	436	0.9	5.4356	5.23

MCNPX DATA CARDS

While every data card in an input deck is important, there are a few that are particularly worth noting for this application. Because coincidence counting is dependent upon the spontaneous fission of nuclear isotopes, the source definition card should specify spontaneous fission. The spontaneous fission source was specified using the par = SF command in the source definition card. This command defines the source particles as spontaneous fission neutrons. For each sample, the spontaneous fission source was defined as the nuclear material cell.

However, as discussed earlier, there are (α,n) neutrons in the samples that induce fission and can lead to distorted count rates. To take this into account, two separate input decks were created: a spontaneous fission input deck and an (α,n) input deck. The (α,n) input deck specified the (α,n) neutron source as defined by SOURCES[13], a code used to

generate neutron source strength and spectra based on isotopic and chemical composition of a material. The neutron source spectrum used for the (α,n) neutron source is shown in Figure 4.4. This (α,n) source was input into MCNPX using the source definition cards. The source was defined in the nuclear material cell based on discrete source energy probabilities (see Appendix A).

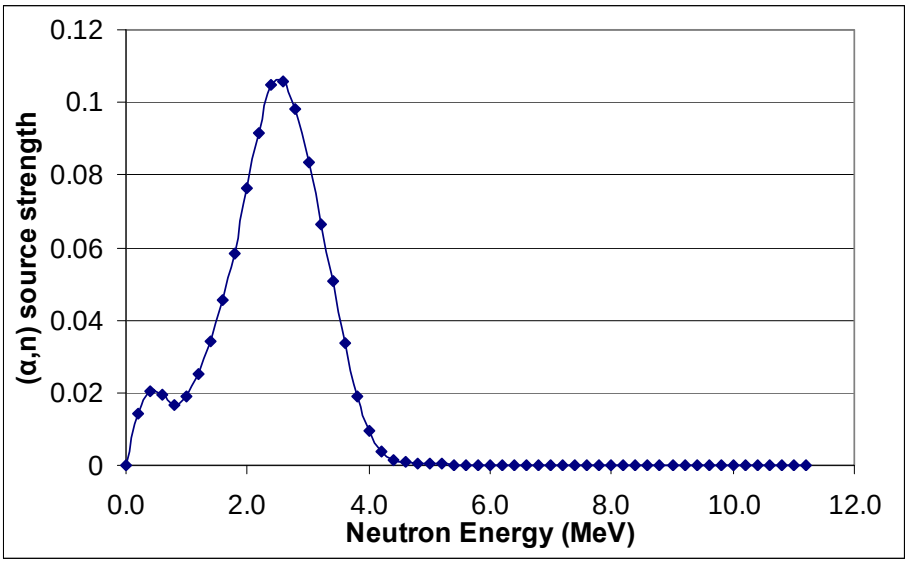

Figure 4.4. (α,n) source spectrum generated by SOURCES.

The tallies used in these MCNPX models are of special importance. A number of tallies were assigned to each input deck. First, a number of F4 tallies, which tally the flux averaged over a specified cell, were included in each deck. This is the traditional tally used to generate the unknown parameters needed for the Neutron Coincidence Point Model. There were five F4 tallies per deck: one tally for each detector slab individually, which summed over all four ^{3}He tubes in that slab, and one tally representing the sum of all four slabs, or all sixteen ^{3}He tubes.

A tally multiplier card was used to calculate the (n,p) reaction in the ^{3}He. A time card was used to set a pre-delay of 4.5 μs and a gate of 64 μs. The upper limit, the time at

which the tally quit counting, was set to 1E10 μs. These tallies, and other data cards, were included in both the spontaneous fission and (α,n) decks.

Second, F8 tallies were included in each input deck. The new MCNPX capabilities discussed earlier are embedded in this F8 tally. The F8 tally is defined as an energy distribution of pulses created in a detector by radiation. Using the FT card, designed to specify special treatment for a given tally, the F8 tally can be used as a neutron coincidence capture tally. The word *cap* is specified after the F8 command. The material in which the capture occurs is listed next. In this case, for example, it would be the ^{3}He. If desired, the gate length can be specified by entering the word *gate* after the capturing material followed by the pre-delay and gate length. If the gate is not specified, it is assumed to be infinite.

This ^{3}He capture tally was implemented twice in each input deck. The first F8 tally was assigned to tally over all four slabs with an infinite gate width. The second F8 tally was assigned a pre-delay and gate-width of 4.5 μs and 64 μs, respectively, and also tallied over all four slab responses.

The ratio of the doubles efficiency with a finite gate to that of an infinite gate leads to the determination of the doubles gate fraction, which is a parameter needed in the point model equations. Thus, a spontaneous fission input deck and an (α,n) input deck were created for each PuO_2 standard measured. A sample of a spontaneous fission deck and an (α,n) deck can be found in Appendix A.

MCNPX OUTPUT

Each MCNPX input deck was executed on a 3.2 GHz Linux machine. Each deck executed one million histories. A separate output file was generated for each input deck.

The singles efficiency is acquired directly from the F4 tallies with the FM multiplier card. These efficiencies already incorporate the self-multiplication in the sample; therefore, it is important that when using them in the point model equations, M is set to unity. The F8 tallies also directly generate the singles efficiencies for each sample. Again, these efficiencies include the self-multiplication in the sample. Tables 4.2 and 4.3 list the singles efficiencies calculated using both the F4 and F8 tallies for the spontaneous fission and (α,n) decks, respectively. Note the results posted here are those generated using the tallies that summed over all detector slabs.

Table 4.2. MCNPX Calculated Singles Efficiencies for Spontaneous Fission Decks.

Sample ID	**F4 Calculated Singles Efficiency (%)**	**F8 Calculated Singles Efficiency (%)**
LAO-251	9.239 ± 0.277	9.244 ± 0.020
LAO-252	9.341 ± 0.028	9.341 ± 0.021
LAO-255	9.522 ± 0.028	9.559 ± 0.021
LAO-256	9.403 ± 0.027	9.398 ± 0.021

Table 4.3. MCNPX Calculated Singles Efficiencies for (α,n) Decks.

Sample ID	**F4 Calculated Singles Efficiency (%)**	**F8 Calculated Singles Efficiency (%)**
LAO-251	7.881 ± 0.035	7.838 ± 0.027
LAO-252	8.003 ± 0.036	7.952 ± 0.028
LAO-255	8.142 ± 0.037	8.104 ± 0.028
LAO-256	8.045 ± 0.036	8.009 ± 0.028

Note that the singles efficiencies calculated for the spontaneous fission deck are higher than those for the (α,n) deck. This is due to the fact that (α,n) neutrons have higher average energies than spontaneous fission neutrons. The PNCC has a lower efficiency for measuring these higher energy neutrons.

The doubles efficiencies were also calculated using the F8 tally and a gate length of 64 μs. Table 4.4 lists the doubles efficiencies calculated for the spontaneous fission and (α,n) decks. Recall that (α,n) neutrons occur in singlets; therefore, no doubles counts should be expected from the (α,n) source. However, (α,n) neutrons can induce fission, which will produce coincidence neutrons. This accounts for the low, but non-zero, doubles efficiency in the (α,n) decks. Note that because the doubles rates are extremely low for the (α,n) case, the uncertainties in the calculated doubles efficiencies are nearly 100 %.

Table 4.4. MCNPX F8 Calculated Doubles Efficiencies for Spontaneous Fission and (α,n) Decks.

Sample ID	**Spontaneous Fission Doubles Efficiency (%)**	**(α,n) Doubles Efficiency (%)**
LAO-251	0.502 ± 0.005	0.043 ± 0.002
LAO-252	0.539 ± 0.006	0.059 ± 0.003
LAO-255	0.589 ± 0.006	0.076 ± 0.003
LAO-256	0.557 ± 0.006	0.063 ± 0.003

Other data that were obtained from the MCNPX output included the self-multiplication and the doubles gate fraction for each sample. Both of these parameters are needed for

the Neutron Coincidence Point Model analysis. Note that the self-multiplication value, M, calculated in MCNPX should be used only when the measured efficiency is used, as it does not take multiplication into account; however, in the calculations discussed here the calculated efficiency was used so the self-multiplication was set to unity.

The doubles gate fraction was also obtained for the MCNPX output. The doubles gate fraction (f_d) was determined using:

$$f_d = \frac{\varepsilon_{\text{finite}}}{\varepsilon_{\text{infinite}}} \quad , \qquad \textit{(Eq. 4.1)}$$

where ε_{finite} is the doubles efficiency using a finite gate length (64 μs), and $\varepsilon_{infinite}$ is the doubles efficiency using an infinite gate length (1E10 μs). The self-multiplication and doubles gate fraction values determined by MCNPX are listed in Table 4.5. Note that the doubles gate fraction calculated using values from the F4 tallies are consistently higher than those using the F8 tallies. This may be the result of the doubles efficiency calculation. For example, the F4 tally does not directly calculate the doubles efficiencies, but using a time card and essentially creating a window, this can be estimated.

Table 4.5. MCNPX Determined Parameters.

Sample ID	f_d (F8)	M (F8)	f_d (F4)
LAO-251	0.581 ± 0.008	1.0725 ± 0.0004	0.607 ± 0.003
LAO-252	0.591 ± 0.008	1.0895 ± 0.0004	0.616 ± 0.003
LAO-255	0.611 ± 0.008	1.1064 ± 0.0004	0.626 ± 0.003
LAO-256	0.597 ± 0.008	1.0953 ± 0.0004	0.621 ± 0.003

RESULTS

Once the data was extracted from the MCNPX output, it was used to calculate the singles and doubles count rates for each sample. The singles count rates (*S)* were calculated using:

$$S = (\varepsilon_{SF} * Y_{SF}) + (\varepsilon_{(\alpha,n)} * Y_{(\alpha,n)}), \qquad \textit{(Eq. 4.2)}$$

where ε_{SF} and $\varepsilon_{(\alpha,n)}$ are the singles efficiencies calculated by the spontaneous fission and (α,n) decks, respectively, and Y_{SF} and $Y_{(\alpha,n)}$ are the spontaneous fission and (α,n) neutron yields for each sample (in n/s), respectively (see Tables 1.1 and 3.5). Table 4.6 lists the singles count rates for each sample calculated using both the F4 and F8 tallies.

Table 4.6. MCNPX Calculated Singles Count Rates.

Sample ID	**F8 Totals Count Rate (cps)**	**F4 Totals Count Rate (cps)**
LAO-251	3973 ± 10	3978 ± 13
LAO-252	7434 ± 19	7448 ± 26
LAO-255	12931 ± 33	12914 ± 43
LAO-256	8949 ± 23	8964 ± 30

The doubles count rates (*D*) were calculated using:

$$D = (\varepsilon_{SF} * Y_{SF}) + (\varepsilon_{(\alpha,n)} * Y_{(\alpha,n)}), \qquad \textit{(Eq. 4.3)}$$

where ε_{SF} and $\varepsilon_{(\alpha,n)}$ are the doubles efficiencies calculated by the spontaneous fission and (α,n) decks, respectively, and Y_{SF} and $Y_{(\alpha,n)}$ are the spontaneous fission and (α,n) neutron yields for each sample (in n/s), respectively (see Tables 1.1 and 3.5). The calculated doubles count rates are shown in Table 4.7.

Table 4.7. MCNPX Calculated Doubles Count Rates.

Sample ID	**F8 Total Count Rate (cps)**
LAO-251	158 ± 2
LAO-252	318 ± 4
LAO-255	595 ± 7
LAO-256	394 ± 5

The singles and doubles rates are plotted in Figure 4.5 and 4.6, respectively. The calculated singles rates from both the F4 and F8 tallies and the doubles count rates calculated using the F8 tallies are plotted against $^{240}Pu_{eff}$ mass. The error bars are included in the plots but are too small to observe.

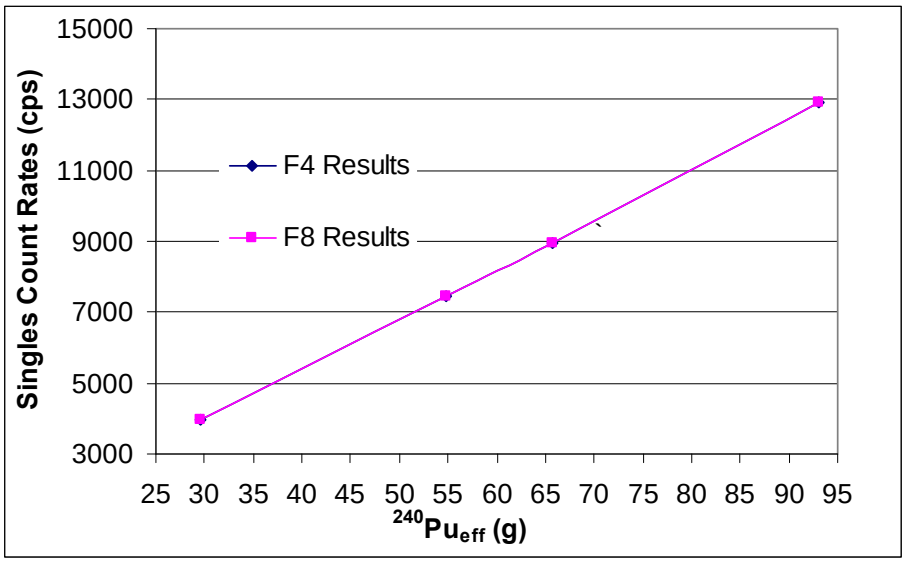

Figure 4.5. MCNPX calculated singles count rates as function of $^{240}Pu_{eff}$ mass.

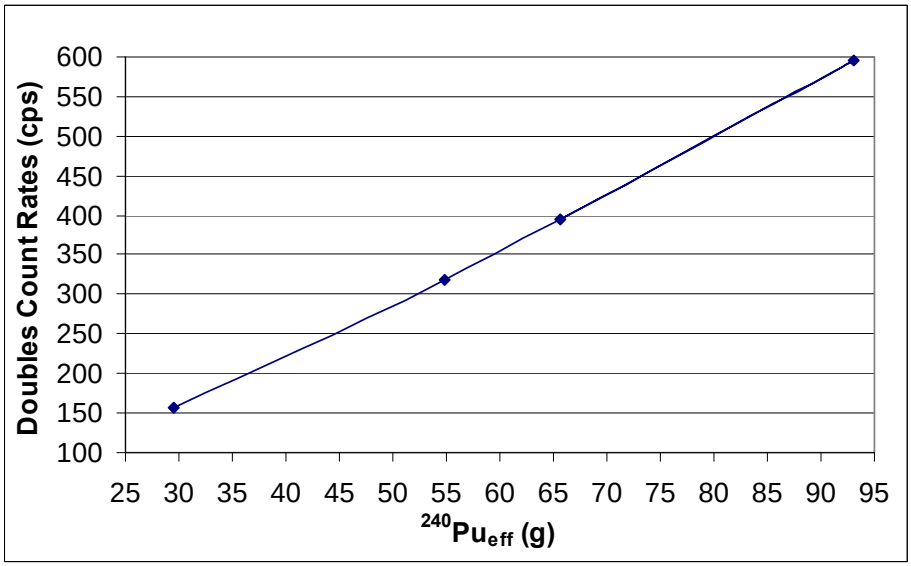

Figure 4.6. MCNPX calculated doubles count rates as a function of $^{240}Pu_{eff}$ mass.

As expected, both the singles and doubles count rates increase with increasing Pu mass. Also note that the singles rates calculated using the F4 and F8 tallies are almost identical.

This implies that the physics behind each tally is consistent. An in-depth comparison between these MCNPX results and the measured data as well as the corresponding discussion follows in Chapter V.

CHAPTER V

DATA ANALYSIS

A major objective in this research was to evaluate the new multiplicity capabilities of MCNPX for neutron coincidence counting analysis. In order to evaluate the potential of this new feature, an in-depth analysis of the PNCC was performed. This study involved measurements of four PuO_2 known standards. These measurements were analyzed using the Neutron Coincidence Point Model. MCNPX was then used to directly calculate the singles and doubles count rates based on a model of the PNCC. A comparison of these different results is discussed below.

NEUTRON COINCIDENCE POINT MODEL RESULTS

As previously mentioned, use of the Neutron Coincidence Point Model equations require more information about a given sample than is typically available. This problem is often addressed through the aid of a computation model such as MCNPX. MCNPX is frequently used to determine the following parameters: the (α,n) to spontaneous fission neutron ratio (α), the sample self-multiplication (M), the doubles gate fraction (f_d), and the efficiency (ε) of the system.

Because the isotopics of the four PuO_2 standards were known, the (α,n) to spontaneous fission neutron ratios for each standard could be calculated. They were calculated using the (α,n) and spontaneous fission neutron yields given in Tables 1.1 and 3.5. The system efficiency was both measured and calculated using MCNPX. The calculated efficiency is listed in Table 5.1, along with the multiplication factor and doubles gate fraction. The self-multiplication and doubles gate fraction for each sample were calculated using the MCNPX F4 tally.

Table 5.1. Neutron Coincidence Point Model
Parameters Calculated Using the MCNPX F4 Tallies.

Sample ID	α	ε	M	f_d
LAO-251	0.502	0.0924 ± 0.0002	1.0725 ± 0.0004	0.607 ± 0.003
LAO-252	0.496	0.0934 ± 0.0002	1.0895 ± 0.0004	0.616 ± 0.003
LAO-255	0.503	0.0952 ± 0.0002	1.1064 ± 0.0004	0.626 ± 0.003
LAO-256	0.494	0.0940 ± 0.0002	1.0953 ± 0.0004	0.621 ± 0.003

Other parameters needed for the point model analysis are listed in Table 5.2. Recall that F is the spontaneous fission rate, m is the ^{240}Pu effective mass, ν_{s1} and ν_{s2} are the first and second reduced moments of the spontaneous fission neutron distribution, and ν_{i1} and ν_{i2} are the first and second reduced moments of the induced fission neutron distribution. These are known parameters, with the exception of the $^{240}Pu_{eff}$ mass, and are constant for any particular isotope, namely ^{240} Pu. However, because these parameters are different for other Pu isotopes, there may be error involved in assuming ^{240}Pu parameters for the entire samples.

Table 5.2. Known Neutron Coincidence Point Model Parameters.

Sample ID	F (fis/s-g(240))	m (g $^{240}Pu_{eff}$)	vs1	vs2	vi1	vi2
LAO-251	473	29.57	2.154	3.789	3.163	8.24
LAO-252	473	54.86	2.154	3.789	3.163	8.24
LAO-255	473	93.02	2.154	3.789	3.163	8.24
LAO-256	473	65.70	2.154	3.789	3.163	8.24

Using these parameters and Equations 1.3 and 1.4, the expected singles and doubles count rates can be calculated. It is important to note that the calculated efficiencies were used and therefore the sample self-multiplication values were set to unity. Table 5.3 shows the expected count rates from the Neutron Coincidence Point Model using the unknown parameters from the MCNPX F4 tallies.

Table 5.4 lists the unknown parameters calculated using the F8 tallies. These F8 parameters were substituted into the Neutron Coincidence Point Model equations. Table 5.5 shows the expected count rates based on these F8 parameters. The only notable difference between these calculated parameters from the two different tallies is the doubles gate fractions.

Table 5.3. Expected Count Rates Based on the Neutron Coincidence Point Model and the F4 Tally Calculated Parameters.

Sample ID	**Calculated Singles Rate (cps)**	**Calculated Doubles Rate (cps)**
LAO-251	4180 ± 13	137 ± 1
LAO-252	7813 ± 23	264 ± 2
LAO-255	13560 ± 39	473 ± 3
LAO-256	9405 ± 27	323 ± 2

Table 5.4. Neutron Coincidence Point Model Parameters Calculated Using the MCNPX F8 Tallies.

Sample ID	α	ε	M	f_d
LAO-251	0.502	0.0924 ± 0.0002	1.0725 ± 0.0004	0.581 ± 0.008
LAO-252	0.496	0.0934 ± 0.0002	1.0895 ± 0.0004	0.591 ± 0.008
LAO-255	0.503	0.0956 ± 0.0002	1.1064 ± 0.0004	0.611 ± 0.008
LAO-256	0.494	0.0940 ± 0.0002	1.0953 ± 0.0004	0.597 ± 0.008

Table 5.5. Expected Count Rates Based on the Neutron Coincidence Point Model and the F8 Tally Calculated Parameters.

Sample ID	Calculated Singles Rate (cps)	Calculated Doubles Rate (cps)
LAO-251	4182 ± 9	132 ± 1
LAO-252	7813 ± 17	254 ± 1
LAO-255	13614 ± 30	465 ± 2
LAO-256	9401 ± 21	310 ± 1

There are no substantial differences in the point model calculated singles rates based on the two sets of MCNPX data. The doubles rates are statistically different because of the difference of the doubles gate fractions. Table 5.6 shows the measured data once again. The calculated singles and doubles rates from the two different sets of data are both similar to the measured count rates. Graphs of the singles and doubles count rates are shown in Figures 5.1 and 5.2, respectively. Again, error bars are included on the plots but are too small to be visible.

Table 5.6. Measured Count Rates for the PuO_2 Standards.

Sample ID	Measured Singles Rate (cps)	Measured Doubles Rate (cps)
LAO-251	3721 ± 3	132 ± 2
LAO-252	7017 ± 3	268 ± 2
LAO-255	12191 ± 4	493 ± 4
LAO-256	8369 ± 4	329 ± 3

From the plots in Figures 5.1 and 5.2, a clear bias error exists in the count rates calculated using the MCNPX parameters. This bias is due to the increased efficiency calculated by MCNPX. The measured efficiency for each sample was approximately 8.4 %, while the MCNPX calculated efficiency was approximately 9.4 %. This error in the efficiency directly translated to this bias error in the calculated count rates.

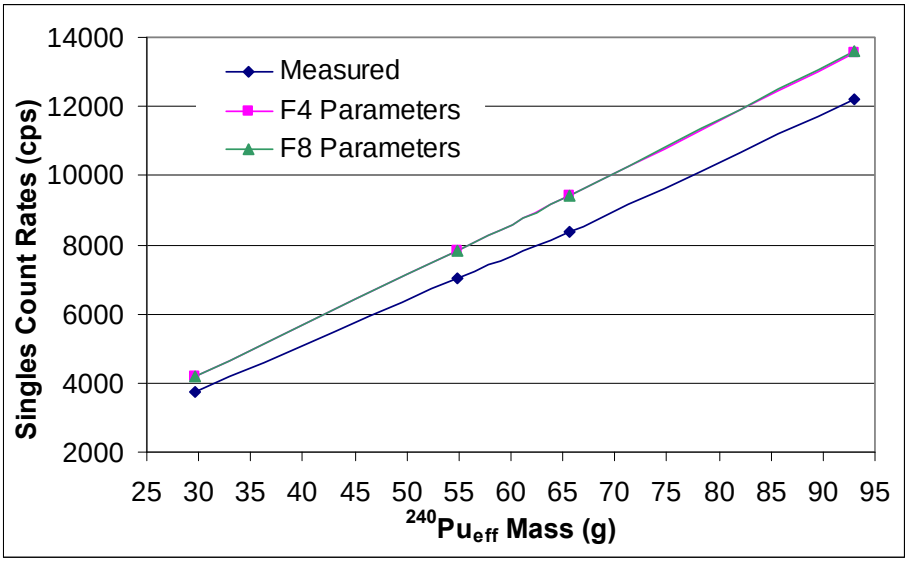

Figure 5.1. Point model calculated singles count rates.

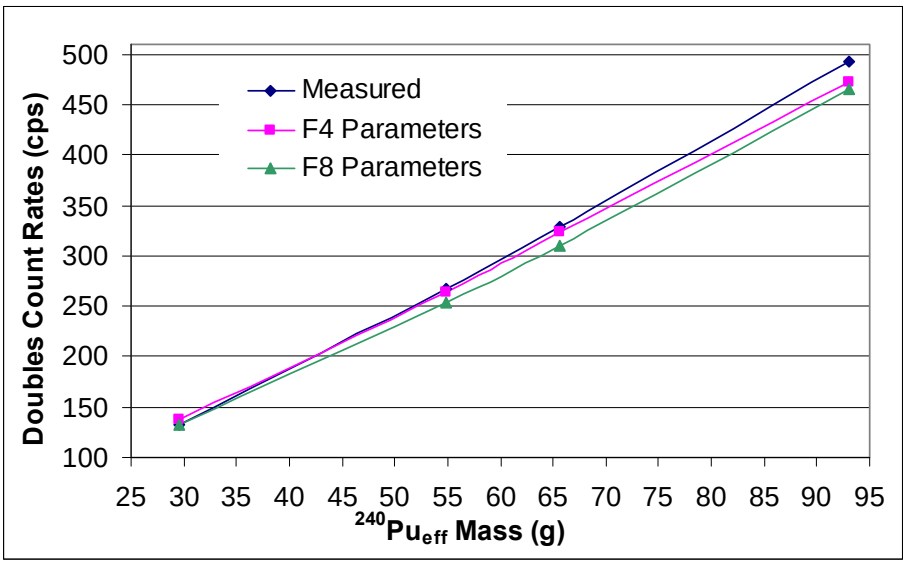

Figure 5.2. Point model calculated doubles count rates.

Table 5.7 lists the statistical differences in the point model results relative to the measured results.

Table 5.7. Point Model Differences Relative to the Measured Results.

Sample ID	F4 Singles Difference (%)	F4 Doubles Difference (%)	F8 Singles Difference (%)	F8 Doubles Difference (%)
LAO-251	12.3%	-3.5%	12.4%	-0.3%
LAO-252	11.3%	-1.5%	11.3%	-5.2%
LAO-255	11.2%	-4.1%	11.7%	-5.7%
LAO-256	12.4%	-1.8%	12.3%	-5.8%

The results from the two different MCNPX tallies are clearly very similar. For the singles rates, the differences in the results based on the F4 data and those based on the

F8 data are hardly distinguishable. Both sets of data are consistently 12 % higher than the measured values. The doubles rates calculated using the F4 data produces results within ~ 4 % of the measured data. The doubles rates from the F8 data are within ~ 6 % of the measured values.

Sources of error in the point model results could involve the uncertainties associated with the PuO_2 standards. These include the unknown density and inner canning dimensions. While the statistical error associated with MCNPX should always be considered, it is very low for these cases. The accuracy of the nuclear data used could be yet another source of error. For the best results, each of these potential sources of error should be minimized.

MCNPX RESULTS

As previously discussed, MCNPX now includes advanced neutron multiplicity capabilities that allow detector responses to be directly calculated. This new capability was explored using the F8 neutron capture tally. As discussed in Chapter IV, the use of this capture tally produces neutron coincidence information that can be used to calculate the doubles count rates in a given detector. The results of these calculations are listed in Tables 4.6 and 4.7.

To compare this data to the measured results, the count rates have again been plotted as a function of $^{240}Pu_{eff}$ mass. The MCNPX singles count rates have been plotted with the measured singles rates in Figure 5.3, while the MCNPX doubles count rates are shown alongside the measured doubles rates in Figure 5.4. Again, the error bars are included on the graphs but are too small to observe.

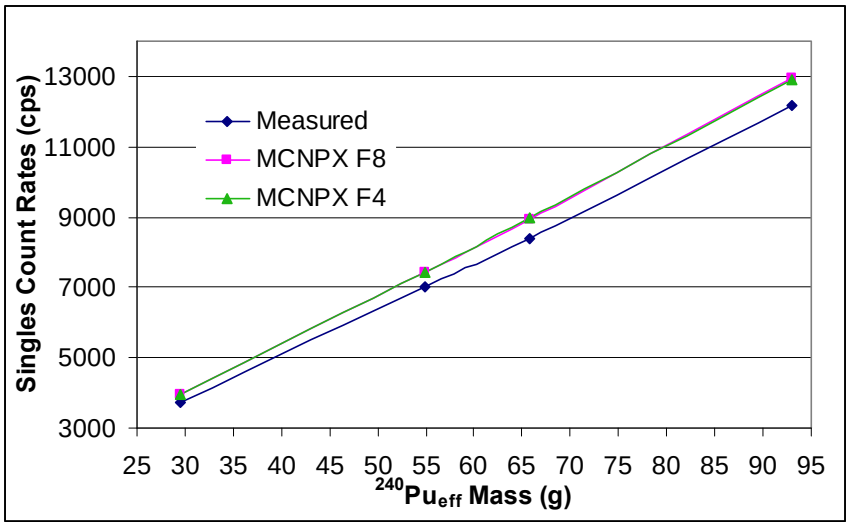

Figure 5.3. MCNPX calculated and measured singles rates as a function of $^{240}Pu_{eff}$ mass for all PuO_2 standards.

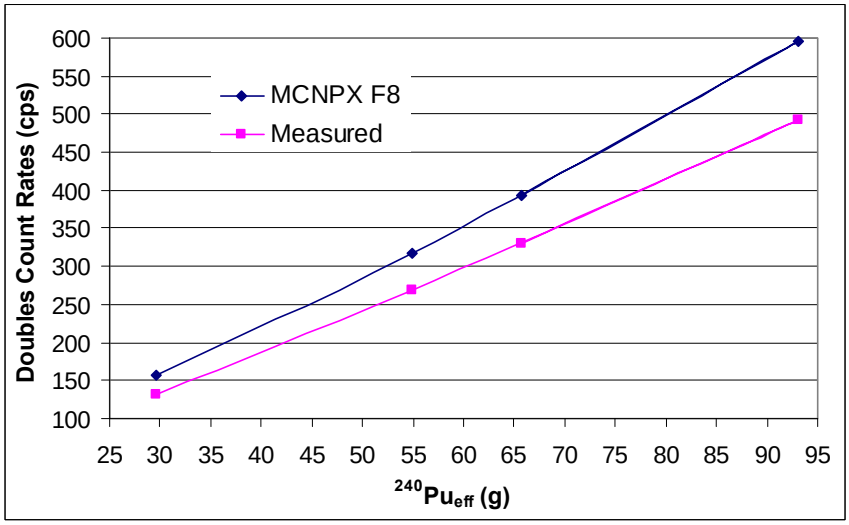

Figure 5.4. MCNPX calculated and measured doubles rates as a function of $^{240}Pu_{eff}$ mass for all PuO_2 standards.

NEUTRON COINCIDENCE POINT MODEL ANALYSIS

Based on Figures 5.1 and 5.2, it is evident that the Neutron Coincidence Point Model does a very good job estimating both the singles and the doubles count rates for various masses of PuO_2. This seems to be true regardless of which tally information was used.

MCNPX ANALYSIS

The results based on the MCNPX calculations differed from those based on the Neutron Coincidence Point Model. The differences between the MCNPX calculated results and the measured results are listed in Table 5.8. The singles count rates determined using MCNPX directly appear to match the measured data well; however, the doubles count rates do not correlate with the measured data as well.

Table 5.8. MCNPX Differences Relative to the Measured Results.

Sample ID	F8 Singles Difference (%)	F4 Singles Difference (%)	F8 Doubles Difference (%)
LAO-251	6.8%	6.9%	19.2%
LAO-252	5.9%	6.1%	18.5%
LAO-255	6.1%	5.9%	20.8%
LAO-256	6.9%	7.1%	19.7%

The differences between the MCNPX singles and the measured singles rates are about 6 %. This is roughly half the difference than that of the point model results. This is the case for both the F4 and F8 results. This implies that the calculation of the singles rates is consistent between the F4 and F8 calculations. The doubles rates, on the other hand,

were not as well matched. The differences in these doubles rates and the measured values were nearly 20 % for each sample.

Numerous effects could cause this deviation from the measured results. The samples that were modeled had many unknown parameters. The density, for example, could in fact differ from the estimated value of 0.9 g/cc. The canning dimensions could be other than those given in Chapter IV. In particular, the effect of the diameter of the sample was not evaluated. The masses and other MCNPX input were checked thoroughly and are not believed to be the source of the error. The important thing to note is that the point model using parameters from MCNPX works better than using MCNPX directly.

CHAPTER VI

SENSITIVITY ANALYSIS

In order to better understand how various sample characteristics affect the PNCC response, a short sensitivity analysis was performed. In this sensitivity analysis, the dependence on sample density and water content was explored. As previously discussed, the density of the material in the sample affects the geometry of the problem as well as the absorption and multiplication properties of the material. The water content in the sample is important because it affects the absorption and multiplication properties of the sample.

DENSITY SENSITIVITY

Although the density of each sample was not known, it was estimated to be 0.9 g/cc. Again, this density was assumed based on the origins of the PuO_2 in the standards. MCNPX was used to determine the effects that various sample densities have on the measured count rates.

MCNPX was used to model the smallest and largest samples, LAO-251 and LAO-255, with densities of 0.7, 0.9, 1.2, and 2.5 g/cc. The MCNPX input decks remained the same as those used to calculate the original count rates, with the exception of the different PuO_2 densities and therefore the different fill height of the nuclear materials. The calculations discussed in Chapter IV were then repeated.

The newly calculated singles rates, in cps, are shown in Table 6.1. Note the highlighted column reflects the data based on the original density assumption of 0.9 g/ cc. Table 6.2 shows doubles rates, in cps, based on the same densities. Again, the highlighted column shows the data based on the original density assumption of 0.9 g/cc.

Table 6.1. Calculated Singles Rates (in cps) Based on Various Sample Densities.

Sample ID	PuO_2 Densities			
	0.7 g/ cc	**0.9 g/ cc**	**1.2 g/ cc**	**2.5 g/ cc**
LAO-251	3955	3973	3985	4014
LAO-255	12981	12931	12927	13039

Table 6.2. Calculated Doubles Rates (in cps) Based on Various sample Densities.

Sample ID	PuO_2 Densities			
	0.7 g/ cc	**0.9 g/ cc**	**1.2 g/ cc**	**2.5 g/ cc**
LAO-251	156	158	159	160
LAO-255	602	595	588	593

The singles count rates differed from the base case of 0.9 g/cc by less than 2 %, while the doubles count rates differed by less than 3 %. To better understand the affect of the sample density, the singles and doubles rates were plotted as a function of density, shown in Figures 6.1 and 6.2 respectively. As can be seen, the PNCC is relatively insensitive to the sample density.

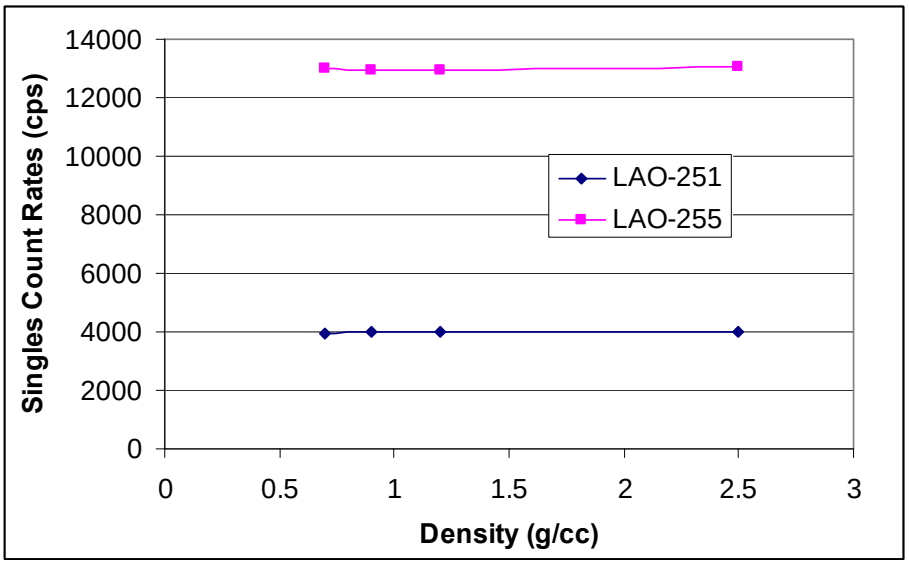

Figure 6.1. Calculated singles rates as a function of sample density.

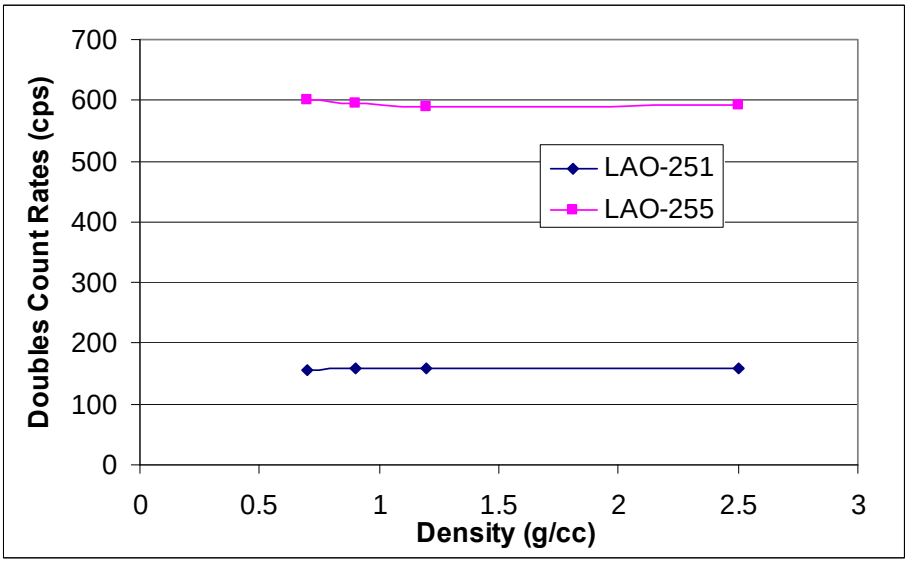

Figure 6.2. Calculated doubles rates as a function of sample density.

To quantify the change in count rate as a function of density, sensitivity parameters were calculated using:

$$S_{\rho 1} = \frac{\%\ change\ in\ S}{\%\ change\ in\ \rho} \quad , \qquad (Eq.\ 6.1)$$

$$S_{\rho 2} = \frac{\%\ change\ in\ D}{\%\ change\ in\ \rho} \quad , \qquad (Eq.\ 6.2)$$

where S is the singles count rate (in cps), D is the doubles count rate (in cps), and ρ is the density of the material in the sample (in g/cc). Table 6.3 shows the averaged parameters for each case. As can be seen, both the singles and doubles count rates are relatively insensitive to variations in sample density. Thus, inspectors would only need a very rough estimate of the sample density when using the PNCC.

Table 6.3. Sensitivity Parameters for Density Analysis.

Sample ID	**S_{D1}**	**S_{D2}**
LAO- 251	0.013	0.030
LAO- 255	0.009	0.030

WATER SENSITIVITY

The PuO_2 standards used to characterize the PNCC were in the form of powder, which tends to draw moisture out of the air. The characterization and analysis in the preceding chapters assumed there was no water in the samples; however, without direct measurement of the water content this remains a possible source of error. A sensitivity analysis was performed to determine how varying water content in a given sample would alter the results measured by the detector system.

Excess water in a sample increases neutron absorption, which is a loss mechanism, but also moderated more neutrons, making them more likely to be detected in the ^{3}He tubes and more likely to have self-multiplication. The additional oxygen in the water also could increase the (α,n) source strength. The water sensitivity analysis was used to determine how these competing mechanisms affect the PNCC response.

MCNPX was again used to evaluate the PNCC sensitivity to water in the samples. The previous models, those used to evaluate the new multiplicity capabilities in MCNPX, were used; however, the nuclear materials in the PuO_2 standards were adjusted to include 0.25, 1.0, 3.0, and 5.0 % water by mass.

The count rates were then calculated using F8 tallies, as explained in Chapter IV. The singles rates calculated for the various water contents can be found in Table 6.4. The highlighted column, the case with 0 % water, is the base case used for all the analysis previously discussed, including the density analysis. The doubles rates, also calculated using F8 tallies, can be found in Table 6.5. Again the highlighted column with 0 % water was the source of the previous analysis and discussion. The statistical errors given in these tables were determined based on the case with 5 % water.

Table 6.4. Calculated Singles Count Rates for Various Sample Water Contents.

Sample ID	**0 % H_20 Singles (cps)**	**0.25 % H_20 Singles (cps)**	**1 % H_20 Singles (cps)**	**3 % H_20 Singles (cps)**	**5 % H_20 Singles (cps)**	**Statistical Error (cps)**
LAO-251	3973	3971	3977	3985	3995	10
LAO-252	7434	7437	7453	7499	7514	19
LAO-255	12931	12936	12968	13061	13148	34
LAO-256	8949	8949	8967	9031	9069	23

Table 6.5. Calculated Doubles Count Rates for Various Sample Water Contents.

Sample ID	0 % H_20 Doubles (cps)	0.25 % H_20 Doubles (cps)	1 % H_20 Doubles (cps)	3 % H_20 Doubles (cps)	5 % H_20 Doubles (cps)	Statistical Error (cps)
LAO-251	158	157	157	157	157	2
LAO-252	318	318	314	319	331	5
LAO-255	595	601	598	607	621	8
LAO-256	394	393	393	403	403	6

The differences between each case and the base case (0 % water) were computed. The differences for the singles rates can be found in Table 6.6, while the differences in the doubles rates can be found in Table 6.7. Note these calculated differences are relative to the MCNPX case with 0 % added water, not the measured results.

Table 6.6. Singles Rate Differences for Various Water Cases Relative to the MCNPX Base Case.

Sample ID	0.25% H_2O Difference (%)	1% H_2O Difference (%)	3% H_2O Difference (%)	5.0% H_2O Difference (%)
LAO-251	0.059%	0.108%	0.303%	0.565%
LAO-252	0.039%	0.254%	0.875%	1.072%
LAO-255	0.040%	0.283%	0.996%	1.652%
LAO-256	0.004%	0.205%	0.912%	1.327%

Table 6.7. Doubles Rate Differences for Various Water Cases Relative to the MCNPX Base Case.

Sample ID	0.25% H_2O Difference (%)	1% H_2O Difference (%)	3% H_2O Difference (%)	5.0% H_2O Difference (%)
LAO-251	0.469%	0.552%	0.355%	0.311%
LAO-252	0.034%	1.028%	0.498%	4.146%
LAO-255	0.940%	0.508%	1.889%	4.196%
LAO-256	0.245%	0.232%	2.171%	2.230%

Based on the MCNPX calculations for the cases without water, the differences in the singles rates are less than 1.7 %. The results of this analysis led to the conclusion that the addition of small amounts of water does not significantly alter the singles rates detected by the PNCC. This is believed to occur because the competing neutron interactions, due to the additional water in the sample, appear to offset one another. The difference in the doubles rate is at most 4.2 % when 5 % additional water is present.

To further quantify the change in count rate as a function of water content, sensitivity parameters were calculated using:

$$S_{W1} = \frac{\%\ change\ in\ S}{\%\ change\ in\ W} \quad , \qquad \textit{(Eq. 6.3)}$$

$$S_{W2} = \frac{\%\ change\ in\ D}{\%\ change\ in\ W} \quad , \qquad \textit{(Eq. 6.4)}$$

where S is the singles rate (in cps), D is the doubles rate (in cps), and W is the water content in the samples. Table 6.8 shows the averaged parameters for each case. Again,

the plot and low sensitivity parameters imply that the water content does not significantly affect the count rates.

Table 6.8. Sensitivity Parameters for Water Analysis.

Sample ID	S_{W1}	S_{W2}
LAO- 251	0.001	0.006
LAO- 252	0.002	0.005
LAO- 255	0.003	0.015
LAO- 256	0.002	0.006

The doubles rates seemed to be driven primarily by the number of neutrons created. To assess this dependence on the number of neutrons created, additional water cases were analyzed using MCNPX. These supplementary cases included adding 0.1, 0.2, 0.25, 1, 3, 5, 10, 20, 40, 60, 80, and 100% water by mass for to the smallest and largest samples. Recall that LAO-251 contains 29.57 g of $^{240}Pu_{eff}$ while LAO-255 contains 93.02 g of $^{240}Pu_{eff}$. The numbers of neutrons both created and lost were recorded and are given in Table 6.9. The results based on the smaller sample are plotted in Figure 6.3. The numbers of neutrons created and lost are plotted as a function of additional water. The equivalent plot for the larger sample is shown in Figure 6.4.

Table 6.9. Numbers of Neutrons Created and Lost for Smallest and Largest PuO_2 Samples.

H_2O Added (%)	LAO-251		LAO-255	
	Neutrons Created	**Neutrons Lost**	**Neutrons Created**	**Neutrons Lost**
0.1	558379	191184	-	-
0.2	558187	191095	146666	46366
0.25	558454	191193	146238	46252
1	561247	192085	146234	46249
3	564838	193462	146804	46531
5	568882	194810	147454	46709
10	581121	199222	149981	47498
20	604809	207605	155382	49479
40	668869	229885	194824	63571
60	737473	254376	298700	99888
80	833224	287617	491102	166891
100	941514	325559	789887	271277

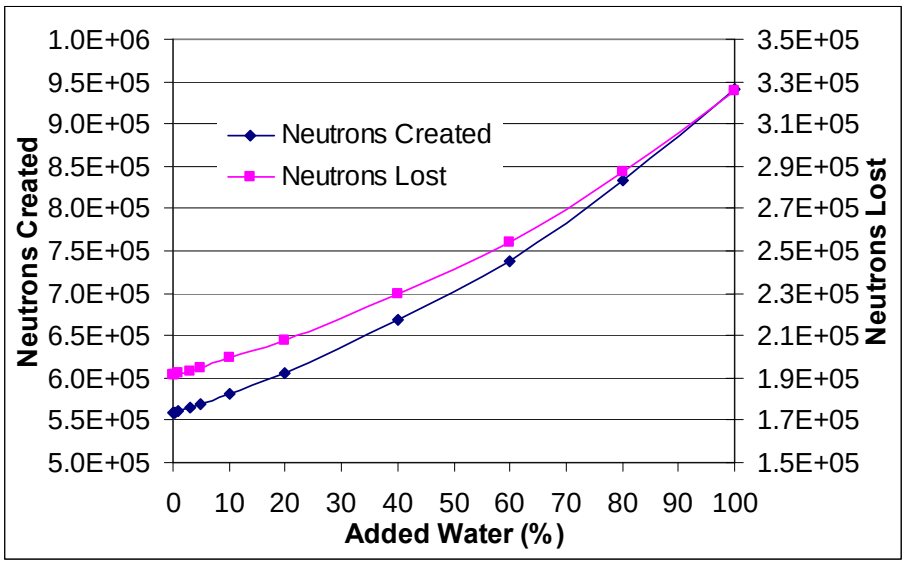

Figure 6.3. Neutron production/loss for LAO-251 PuO_2 standard.

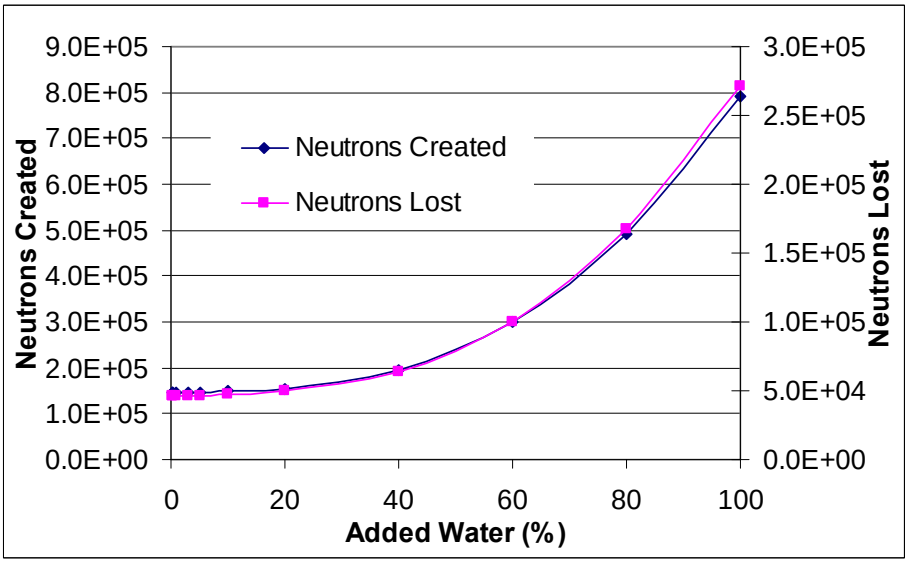

Figure 6.4. Neutron production/loss for LAO-255 PuO_2 standard.

The flat regions of the curves imply that both neutron production and loss are fairly constant for low amounts of additional water. This trend is much more pronounced for

the larger sample, where the number of neutrons created (and lost) did not change significantly until the amount of water added approached 10 %. For the smaller sample, significant changes were not observed until the amount of water added approached 5 %.

Based on these results, it is believed that the competing neutron interactions indeed offset each other. The PNCC appears to be relatively insensitive to small amounts of additional water. At any rate, because the PuO_2 powder can absorb only small quantities of water, it is concluded that the results will not be compromised because of varying water content. Therefore, inspectors would not need to be concerned with water content when using the PNCC as long as the samples were not in any type of solution or wet powder.

CHAPTER VII

CONCLUSION

In summary, the Portable Neutron Coincidence Counter, developed at Los Alamos National Laboratory, was characterized to aid in the verification of nuclear material in various laboratory and field environments. The characterization of the PNCC involved the determination of the detector efficiency and high-voltage plateau, and verification of the symmetry of the system. Once established, the PNCC was used to perform coincidence (or doubles) counting on a series of known PuO_2 standards with varying Pu contents.

The neutron coincidence counting analysis for this system was performed using the Neutron Coincidence Point Model and the new advanced multiplicity capabilities in MCNPX. The two methods of analysis were then compared to determine if MCNPX could accurately simulate the detector response and whether or not it is justifiable to eliminate the use of the point model in neutron coincidence counting analysis altogether.

A brief sensitivity analysis was performed using MCNPX. The sensitivity analysis aimed to determine how varying sample density and water content would affect the detector response. These variables are typically unknown in field applications, so it was important to understand how slight variations could affect the detector results.

DISCUSSION

Characterization

The characterization of the PNCC provided useful information about the system. An efficiency of 8.9 % was measured at the center of the sample volume. Although traditional well counters have efficiencies around 12 %, they are by no means portable. For being a small and portable detector that can be setup to fit an IAEA inspectors

individual needs in virtually any environment, the PNCC has a very acceptable efficiency.

It is important to operate on the high voltage plateau to ensure that the system is insensitive to slight drifts in discrimination levels. The high voltage plateau occurs at approximately 1680 V. While the high voltage is dependent upon the detector itself, the typical range of operating high voltage for radiation detectors is between 700- 1800 V. The high voltage for the PNCC is within the general range.

Repeatability is very important for experimental measurements. Because the system was designed so that the four individual detector slabs could be readily interchanged, they must all have the same response, regardless of location. This helps to ensure that the radiation is measured accurately. As shown in Chapter III, the system is symmetric in the x- and y- directions. For the vertical z- direction, the system is slightly asymmetric. This is expected, however, because the leakage of neutrons is higher at the top of the volume area and the reflection of neutrons is higher at the bottom of the volume area, where the bottom polyethylene slab is positioned.

Measurements

The PuO_2 measurements led to the creation of the reference model for the PNCC. This reference model will allow IAEA inspectors to quantify the amount of $^{240}Pu_{eff}$ in bulk samples immediately after a measurement with the PNCC. The measurements involving the PuO_2 standards also provided a basis for which the Neutron Coincidence Point Model and the MCNPX simulation could be compared.

The measured count rates followed some expected trends. The count rates, both singles and doubles, increased as the amount of $^{240}Pu_{eff}$ increased; the increased amount of nuclear material produced more fissions, and thereby more neutrons. Also, the singles rates were much larger than the coincidence rates. This was expected because the probability of detecting coincident neutrons is much lower than single neutrons.

Although the statistical error for the measurements was very low, other potential sources of error should be considered. One potential source of error was the environmental background. The measurements were performed in a room where many other Pu sources were constantly moved around. While the detector was somewhat shielded, the neutron background may have fluctuated. This source of error, however, may be present in the environments where the PNCC will be used; there is no sure way to avoid it. There may also be error associated with the reference model because of electronic noise, sample uncertainties, and experimental error.

Neutron Coincidence Point Model

The Neutron Coincidence Point Model is the traditional method used in coincidence counting analysis. While many of the parameters needed in the point model equations are known, there are a few unknowns. Typically, an MCNPX model is created to generate these unknown parameters, which are fed back into the point model equations.

Based on the results and analysis discussed in Chapter V, it is obvious that the Neutron Coincidence Point Model does a very good job estimating the doubles rates. This is expected, as the point model is the accepted method for neutron coincidence counting. Although the differences between the measured and calculated singles rates are close to 12 %, the differences between the measured doubles rates and the calculated doubles rates are less than 6 %. For neutron coincidence counting applications performed with the PNCC, a 6 % variation corresponds to roughly 3 grams of ^{240}Pu, based on the plot shown in Figure 5.2. Depending on the level of accuracy needed this may or may not be acceptable.

Another interesting observation was made during this analysis. In general, for the doubles rates, the point model results using the parameters calculated with the traditional F4 tallies appear to be slightly more accurate than the results using the parameters calculated with the new F8 tallies; however, both sets of data are fairly consistent. The

singles rates are comparable for both sets of data. This implication will be further discussed in the next section.

Sources of error in the Neutron Coincidence Point Model include statistical error from Monte Carlo simulations and uncertainties based on nuclear data values used in the point model equations. While nuclear data values tend to be fairly accurate, and for the purposes of this research were assumed to be errorless, MCNPX simulations are only as accurate as the data entered. For example, the density was an unknown factor in the MCNPX model. The uncertainties in these values propagate through to the calculated parameters. There also a number of assumptions embedded in the point model that could lead to additional error.

MCNPX Model

One main goal of this research was to show that MCNPX is now capable of simulating detector response directly; meaning that coincidence counting analysis can now be performed using MCNPX, eliminating the need for the Neutron Coincidence Point Model. The MCNPX results were calculated by taking advantage of the new multiplicity capabilities embedded within. This new ability is exploited using a ^{3}He capture tally which reports both the totals rates and the coincidence rates based on a pre-defined gate width.

The singles rates calculated directly in MCNPX were only different from the measured results by about 6 %. These results are better (by a factor of 2) than the calculated results based on the point model. Interestingly, the MCNPX doubles rates were extremely high. The doubles rates were different from the measured results by roughly 20 %, much worse than the point model results. There seems to be a bias in the doubles results. Based on the plot in Figure 5.4, a 20 % difference in the doubles count rate could result in a 10 g misestimate of ^{240}Pu. This calculation is based on the linearity of the plot. Again, depending on the accuracy needed this may or may not be acceptable.

The MCNPX calculated singles and doubles rates show the expected trends; the count rates increase and diverge from the measured results with increasing $^{240}Pu_{eff}$ mass; however, the MCNPX calculated doubles rates are systematically high by 20 % at each point. Again, the MCNPX calculated singles rates match the measured data better than the point model calculated singles rates.

Another interesting observation is that the singles rates directly calculated using the MCNPX F4 and the F8 tallies are very close. Recall that this is also the case for the point model calculations where the singles rates based on F4 and F8 tally parameters matched. This implies that the singles rate calculation in the F4 and F8 tally is consistent.

The doubles rates calculated with MCNPX, however, appear to have a systematic bias. For each calculated value, the difference relative to the measured result is roughly 20 %. The doubles rates calculated with the point model using parameters from the F4 and F8 tallies are consistently good. Recall that the parameters generated using the F4 and F8 tallies are based on the singles calculations, not the doubles calculations. The only case where the doubles rates are significantly different from the measured rates is when the doubles rates are directly calculated using the F8 tally. This implies that there is an error in the way MCNPX is directly calculating these double rates in the F8 tally.

Sensitivity Analysis

To help pinpoint the cause of the high doubles rates calculated by MCNPX, a sensitivity analysis was performed. This sensitivity analysis focused on varying material densities and water contents of the samples measured. For PuO_2 densities of 0.7, 0.9, 1.2, and 2.5 g/cc, the doubles rates were less than 3 % different than the measured doubles rates. This corresponds to less than 2 grams of ^{240}Pu. Based on this evidence, the density analysis showed that small changes in density do not significantly affect the results of the system.

The water content analysis showed that small additions of water in the PuO_2 samples will not cause significant variations in the measured results. Based on the addition of up to 5 % water, the doubles rates remain within 5 % of the measured rates. A 5 % difference in doubles rates corresponds to less than 3 grams of ^{240}Pu. Further calculations showed that the nuclear reactions competing against each other offset one another for small additions of water.

This sensitivity analysis helps rule out a few potential causes of the very high MCNPX doubles rates. The density analysis showed high doubles rates for each case. This implies that the error does not lie in the density parameter of the model. The water analysis showed the same results. It can therefore be concluded that the error in the MCNPX calculation of the doubles rates lies somewhere other than these input sample characteristics.

In field applications, the sample will generally not be well known. Characteristics such as sample density and water content will not be known. Therefore, it is important that slight variations in wither parameter not affect the integrity of the results.

Method Comparison

As stated earlier, a major goal of this research was to compare the fundamentals of the Neutron Coincidence Point Model to the new multiplicity capabilities in MCNPX. Based on the data analysis above, it is obvious that the Neutron Coincidence Point Model is the best method for neutron coincidence counting applications. Although the singles rates were better calculated using MCNPX, it is the doubles signature that leads to $^{240}Pu_{eff}$ quantification in bulk samples. The doubles rates estimated using the point model far surpassed the doubles rates calculated with MCNPX; however, if the source of error in the MCNPX f8 doubles rate calculation was discovered and corrected, the MCNPX simulation would suffice as a neutron coincidence counting analysis method.

CONCLUSIONS

Given its relatively high efficiency, the PNCC will prove to be a useful tool for neutron coincidence counting. The portability of the system lends itself to many applications in the nuclear field. The creation of the reference model for the PNCC will allow inspectors to quickly verify nuclear samples in a wide range of nuclear environments.

Although the Neutron Coincidence Point Model has proven to be a more accurate method for neutron coincidence analysis, it is evident that MCNPX will be a viable tool that could be utilized for the purposed of neutron coincidence measurements, provided the source of the high doubles rates estimates is located and corrected. Not only will MCNPX be a practical tool, it will be an efficient way to directly simulate detector response.

More work should be done to pinpoint the cause of the high doubles rates calculated using MCNPX. The method used by MCNPX to simulate the doubles rates in the ^{3}He should be revisited. The nuclear data used by the F8 tally should also be reevaluated. If this error was corrected, MCNPX would be an acceptable replacement for the traditional Neutron Coincidence Point Model.

It would also be useful to measure more known standards to check the reference model and to obtain a more accurate interpolation for the reference model of the PNCC. Although the calculations were performed in MCNPX, samples with various masses, densities, and water contents should be measured to evaluate the true sensitivity of the detector system.

REFERENCES

1. D. REILLY, N. ENSSLIN, and H. SMITH, *Passive Nondestructive Assay of Nuclear Materials,* NUREG/CR-5550, U.S. Government Printing Office, Washington, D.C. (1991).

2. S. T. HSUE, J. E. STEWART, T. E. SAMPSON, G. BUTLER, C. R. RUDY, and P. M. RINARD, "Guide to Nondestructive Assay Standards: Preparation Criteria, Availability, And Practical Considerations," LA-13340-MS, Los Alamos National Laboratory report (1997).

3. H. O. MENLOVE, R. ABEDIN-ZADEH, and R. ZHU, "The Analysis of Neutron Coincidence Data to Verify Both Spontaneous Fission and Fissionable Isotopes," LA-11639-MS, Los Alamos National Laboratory Report (1989).

4. Table of Nuclides, http://atom.kaeri.re.kr/, Nuclear Data Evaluation Laboratory, Korea Atomic Energy Research Institute (2007).

5. G. F. KNOLL, *Radiation Detection and Measurement,* 3rd ed., John Wiley and Sons, Inc., Hoboken, New Jersey (2000).

6. N. ENSSLIN, W. C. HARKER, M. S. KRICK, D. G. LANGNER, M. M. PICKRELL, and J. E. STEWART, "Application Guide to Neutron Multiplicity Counting," LA-13422-M, Los Alamos National Laboratory Report (1998).

7. M. ZENDEL, and M. MOESLINGER, "IAEA Safeguards Equipment", http://www.bnl.gov/ISPO/BNLWorkshop07/Presentations/Zendel_Moeslinger.pdf, Brookhaven ISPO Workshop (2007).

8. D. PELOWITZ, Ed., "MCNPX User's Manual," Version 2.5.0, LA-CP-05-0369, Los Alamos National Laboratory Document (2005).

9. ORTEC, "Neutron Coincidence Counting Software," http://ortec-online.com/software/incc-b32.htm, (2007).

10. M. C. MILLER, H. O. MENLOVE, A. L. THORNTON, C. D. RAEL, and L. K. FULTON, "A Portable Neutron Counter for Field Surveys and Assay," LA-UR-05-3492, Los Alamos National Laboratory Document (2005).

11. WHITE ROCK SCIENCE, "SABRINA User's Manual," http://www.whiterockscience.com/sabrina/sabrina.html, (2006).

12. MCNP-VISED 4C2, http://www.rist.or.jp/rsicc/app/MCNP-VISEd4C2.html, (2006).

13. W. B. WILSON, R. T. PERRY, and W. S. CHARLTON, "SOURCES: A Code for Calculating (α, n), Spontaneous Fission, and Delayed Neutron Sources and Spectra," LA-UR-03-1208, Los Alamos National Laboratory Document (2003).

APPENDIX A

(A,N) INPUT DECK

```
MCNP Project (HANDHELD)
c     - cell card -
1   11 -0.96     18  21  24  27       u=1   imp:n=1  $poly box
2   14 -0.001293    -18  19           u=1   imp:n=1  $air space
3   14 -0.001293    -21  22           u=1   imp:n=1  $air space
4   14 -0.001293    -24  25           u=1   imp:n=1  $air space
5   14 -0.001293    -27  28           u=1   imp:n=1  $air space
6   12 -2.70        -19  20  31  32   u=1   imp:n=1  $Al clad
7   12 -2.70        -22  23  33  34   u=1   imp:n=1  $Al clad
8   12 -2.70        -25  26  35  36   u=1   imp:n=1  $Al clad
9   12 -2.70        -28  29  37  38   u=1   imp:n=1  $Al clad
10  13  2.4463e-4   -20                u=1   imp:n=1  $active He tube
11  13  2.4463e-4   -23                u=1   imp:n=1  $active He tube
12  13  2.4463e-4   -26                u=1   imp:n=1  $active He tube
13  13  2.4463e-4   -29                u=1   imp:n=1  $active He tube
14   0                  30                                    imp:n=0
$outside universe
15  14 -0.001293    -30 #24 #25 #26 #33 #34
                        #31 #32 #27 #36 #30 imp:n=1  $sphere
16  13  2.4463e-4   -31                u=1   imp:n=1  $inactive length
17  13  2.4463e-4   -32                u=1   imp:n=1  $inactive length
18  13  2.4463e-4   -33                u=1   imp:n=1  $inactive length
19  13  2.4463e-4   -34                u=1   imp:n=1  $inactive length
20  13  2.4463e-4   -35                u=1   imp:n=1  $inactive length
21  13  2.4463e-4   -36                u=1   imp:n=1  $inactive length
22  13  2.4463e-4   -37                u=1   imp:n=1  $inactive length
23  13  2.4463e-4   -38                u=1   imp:n=1  $inactive length
24   0              -17     fill=1           imp:n=1  $poly box w/ tubes
25  like 24 but trcl=(0 0 0  -1 0 0  0 -1 0  0 0 1) imp:n=1  $opp tubes
26  like 24 but trcl=(0 0 0  0 -1 0  1 0 0  0 0 1)  imp:n=1  $tube slab
27  like 24 but trcl=(0 0 0  0 1 0  -1 0 0  0 0 1)  imp:n=1  $pol/tubes
c   29  15 -2.5        -41  42                      imp:n=1  $glass jar
30  16 -0.900          -42 -43                      imp:n=1  $Pu mix
c   35  18 -10e-20     -45 46 -47 48 -49 50         imp:n=1  $Cf-252
31  17 -2.0            -44                          imp:n=1  $metal top
32 like 31 but trcl=(0 0 0  -1 0 0  0 -1 0  0 0 1)  imp:n=1  $metal top
33 like 31 but trcl=(0 0 0  0 -1 0  1 0 0  0 0 1)   imp:n=1  $metal top
34 like 31 but trcl=(0 0 0  0 1 0  -1 0 0  0 0 1)   imp:n=1  $metal top
36 11 -0.96  -51                                    imp:n=1  $bot poly

c     - surface cards -
17 BOX  -16.51 -8.89 -11.43   7.62 0 0   0 17.78 0   0 0 22.86
18 RCC  -12.7  -5.953 -11.43   0 0 22.86   1.42875    $void hole
19 RCC  -12.7  -5.953 -11.43   0 0 22.86   1.27       $Al clad cylinder
20 RCC  -12.7  -5.953 -8.890   0 0 17.78   1.19380    $He cylinder
21 RCC  -12.7  -1.984 -11.43   0 0 22.86   1.42875    $void hole
22 RCC  -12.7  -1.984 -11.43   0 0 22.86   1.27       $void hole
```

```
23 RCC  -12.7  -1.984 -8.890   0 0 17.78   1.19380    $He cylinder
24 RCC  -12.7   1.984 -11.43   0 0 22.86   1.42875    $void hole
25 RCC  -12.7   1.984 -11.43   0 0 22.86   1.27       $Al clad cylinder
26 RCC  -12.7   1.984 -8.890   0 0 17.78   1.19380    $He cylinder
27 RCC  -12.7   5.953 -11.43   0 0 22.86   1.42875    $void hole
28 RCC  -12.7   5.953 -11.43   0 0 22.86   1.27       $Al clad cylinder
29 RCC  -12.7   5.953 -8.890   0 0 17.78   1.19380    $He cylinder
30 SPH   0 0 0 40
31 RCC  -12.7 -5.953  8.890   0 0 2.540   1.19380     $inactive length
32 RCC  -12.7 -5.953 -11.43   0 0 2.540   1.19380     $inactive length
33 RCC  -12.7 -1.984  8.890   0 0 2.540   1.19380     $inactive length
34 RCC  -12.7 -1.984 -11.43   0 0 2.540   1.19380     $inactive length
35 RCC  -12.7  1.984  8.890   0 0 2.540   1.19380     $inactive length
36 RCC  -12.7  1.984 -11.43   0 0 2.540   1.19380     $inactive length
37 RCC  -12.7  5.953  8.890   0 0 2.540   1.19380     $inactive length
38 RCC  -12.7  5.953 -11.43   0 0 2.540   1.19380     $inactive length
39 BOX  -16.51 8.900 -11.43   26.035 0 0   0 5.08 0   0 0 22.86
40 BOX  -16.51 -13.97 -13.97   26.035 0 0   0 27.94 0   0 0 2.54
41 RCC   0 0 -3.81   0 0 15.24   3.81
42 RCC   0 0 -10.666   0 0 2.33345133      5.4356     $Pu cylinder
43 PZ   -8.33254867                                   $Pu cylinder
44 BOX  -16.51 -8.89 11.43   7.62 0 0   0 17.78 0   0 0 2.54
45 PZ   11.43
46 PZ  -11.43
47 PX   8.89
48 PX  -8.89
49 PY   8.89
50 PY  -8.89
51 BOX -22.51 -17.31 -11.43  46.02 0 0  0 34.32 0  0 0 -5.08 $Poly slab

c     - data cards -
mode n
print
sdef   pos=0 0 -9.499274335 axs=0 0 1 rad=d2 ext=d3 erg=d1
si2    0 5.4356
si3   -1.166725665 1.166725665
c     si1    H
c     sp1   -3  0.799 4.903
c       PuO2 (a,n) Spectrum, calculated.  DHB '05
si1  h 0.00E+00 2.00E-01 4.00E-01 6.00E-01 8.00E-01 1.00E+00
       1.20E+00 1.40E+00 1.60E+00 1.80E+00 2.00E+00 2.20E+00
       2.40E+00 2.60E+00 2.80E+00 3.00E+00 3.20E+00 3.40E+00
       3.60E+00 3.80E+00 4.00E+00 4.20E+00 4.40E+00 4.60E+00
       4.80E+00 5.00E+00 5.20E+00 5.40E+00 5.60E+00 5.80E+00
       6.00E+00 6.20E+00 6.40E+00 6.60E+00 6.80E+00 7.00E+00
       7.20E+00 7.40E+00 7.60E+00 7.80E+00 8.00E+00 8.20E+00
       8.40E+00 8.60E+00 8.80E+00 9.00E+00 9.20E+00 9.40E+00
       9.60E+00 9.80E+00 1.00E+01 1.02E+01 1.04E+01 1.06E+01
       1.08E+01 1.10E+01 1.12E+01
sp1  d 0 1.40E-02 2.02E-02 1.93E-02 1.67E-02 1.89E-02 2.52E-02
         3.42E-02 4.54E-02 5.84E-02 7.62E-02 9.14E-02 1.05E-01
         1.06E-01 9.80E-02 8.36E-02 6.64E-02 5.08E-02 3.39E-02
         1.88E-02 9.46E-03 3.63E-03 1.39E-03 9.54E-04 7.04E-04
         5.53E-04 3.74E-04 2.08E-04 3.57E-05 3.40E-06 3.57E-08
```

```
         0.00E+00 0.00E+00 0.00E+00 0.00E+00 0.00E+00 0.00E+00
         0.00E+00 0.00E+00 0.00E+00 0.00E+00 0.00E+00 0.00E+00
         0.00E+00 0.00E+00 0.00E+00 0.00E+00 0.00E+00 0.00E+00
         0.00E+00 0.00E+00 0.00E+00 0.00E+00 0.00E+00 0.00E+00
         0.00E+00 0.00E+00
fq0   e t f
f4:n  10 11 12 13 t
fm4   -1 13 103
sd4    1 1 1 1 1
t4     450 6850 1E12
f14:n ((10 11 12 13) < 24)
fm14   -1 13 103
sd14    1
f24:n ((10 11 12 13) < 25)
fm24   -1 13 103
sd24    1
f34:n ((10 11 12 13) < 26)
fm34   -1 13 103
sd34    1
f44:n ((10 11 12 13) < 27)
fm44   -1 13 103
sd44    1
f8:n  10 11 12 13 t
ft8   cap 2003
f18:n  (10 11 12 13)
ft18  cap 2003 gate 450 6400
c     t4   300 1100 1900 3500 6700 13100
m11    6000.66c 0.333 1001.60c 0.667         $HDPE density=0.96 g/cm3
mt11   poly.01t
m12   13027.66c 1.000                       $Al   density=2.70 g/cm3
m13    2003.66c 1.000               $He-3,10 atm,den=2.4463e-4 at/barn-
cm
m14    8016.66c 0.210 7014.60c 0.790         $air
m15   14000.60c 0.334 8016.60c 0.666         $glass
m16   94238.66c -0.00048891
      94239.66c -0.72910337
      94240.66c -0.14524399
      94241.66c -0.00412629
      94242.66c -0.00306266
      95241.66c -0.00846288
       8016.66c -0.11797470
c      1001.66c -                          $Pu mix sample
m17   26000.55c 1                          $Iron box
m18   98252.66c 1.000                      $Cf-252 source density 10e-20
nps   1000000
```

SPONTANEOUS FISSION INPUT DECK

```
MCNP Project (HANDHELD)
c     - cell card -
1   11 -0.96     18  21  24  27       u=1   imp:n=1  $poly box
2   14 -0.001293    -18  19           u=1   imp:n=1  $air space
3   14 -0.001293    -21  22           u=1   imp:n=1  $air space
4   14 -0.001293    -24  25           u=1   imp:n=1  $air space
5   14 -0.001293    -27  28           u=1   imp:n=1  $air space
6   12 -2.70        -19  20  31  32   u=1   imp:n=1  $Al clad
7   12 -2.70        -22  23  33  34   u=1   imp:n=1  $Al clad
8   12 -2.70        -25  26  35  36   u=1   imp:n=1  $Al clad
9   12 -2.70        -28  29  37  38   u=1   imp:n=1  $Al clad
10  13  2.4463e-4   -20              u=1   imp:n=1  $active He tube
11  13  2.4463e-4   -23              u=1   imp:n=1  $active He tube
12  13  2.4463e-4   -26              u=1   imp:n=1  $active He tube
13  13  2.4463e-4   -29              u=1   imp:n=1  $active He tube
14   0               30                    imp:n=0  $outside universe
15  14 -0.001293    -30 #24 #25 #26 #33 #34
                        #31 #32 #27 #36 #30 imp:n=1  $sphere
16  13  2.4463e-4   -31              u=1   imp:n=1  $inactive length
17  13  2.4463e-4   -32              u=1   imp:n=1  $inactive length
18  13  2.4463e-4   -33              u=1   imp:n=1  $inactive length
19  13  2.4463e-4   -34              u=1   imp:n=1  $inactive length
20  13  2.4463e-4   -35              u=1   imp:n=1  $inactive length
21  13  2.4463e-4   -36              u=1   imp:n=1  $inactive length
22  13  2.4463e-4   -37              u=1   imp:n=1  $inactive length
23  13  2.4463e-4   -38              u=1   imp:n=1  $inactive length
24   0              -17     fill=1          imp:n=1  $poly box w/ tubes
25  like 24 but trcl=(0 0 0  -1 0 0  0 -1 0  0 0 1) imp:n=1  $opp tubes
26  like 24 but trcl=(0 0 0  0 -1 0  1 0 0  0 0 1)  imp:n=1  $poly/tube
27  like 24 but trcl=(0 0 0  0 1 0  -1 0 0  0 0 1)  imp:n=1  $poly/tube
c   29  15 -2.5        -41  42                      imp:n=1  $glass jar
30  16 -0.900         -42 -43                      imp:n=1  $Pu mix
c   35  18 -10e-20     -45 46 -47 48 -49 50         imp:n=1  $Cf-252
31  17 -2.0           -44                          imp:n=1  $metal top
32 like 31 but trcl=(0 0 0  -1 0 0  0 -1 0  0 0 1)  imp:n=1  $metal top
33 like 31 but trcl=(0 0 0  0 -1 0  1 0 0  0 0 1)   imp:n=1  $metal top
34 like 31 but trcl=(0 0 0  0 1 0  -1 0 0  0 0 1)   imp:n=1  $metal top
36 11 -0.96  -51                                   imp:n=1  $bot slab

c     - surface cards -
17 BOX  -16.51 -8.89 -11.43   7.62 0 0   0 17.78 0   0 0 22.86
18 RCC  -12.7  -5.953 -11.43   0 0 22.86   1.42875    $void hole
19 RCC  -12.7  -5.953 -11.43   0 0 22.86   1.27       $Al clad cylinder
20 RCC  -12.7  -5.953 -8.890   0 0 17.78   1.19380    $He cylinder
21 RCC  -12.7  -1.984 -11.43   0 0 22.86   1.42875    $void hole
22 RCC  -12.7  -1.984 -11.43   0 0 22.86   1.27       $void hole
23 RCC  -12.7  -1.984 -8.890   0 0 17.78   1.19380    $He cylinder
24 RCC  -12.7   1.984 -11.43   0 0 22.86   1.42875    $void hole
25 RCC  -12.7   1.984 -11.43   0 0 22.86   1.27       $Al clad cylinder
26 RCC  -12.7   1.984 -8.890   0 0 17.78   1.19380    $He cylinder
```

```
27 RCC  -12.7   5.953 -11.43   0 0 22.86   1.42875    $void hole
28 RCC  -12.7   5.953 -11.43   0 0 22.86   1.27       $Al clad cylinder
29 RCC  -12.7   5.953 -8.890   0 0 17.78   1.19380    $He cylinder
30 SPH   0 0 0 40
31 RCC  -12.7 -5.953  8.890   0 0 2.540   1.19380     $inactive length
32 RCC  -12.7 -5.953 -11.43   0 0 2.540   1.19380     $inactive length
33 RCC  -12.7 -1.984  8.890   0 0 2.540   1.19380     $inactive length
34 RCC  -12.7 -1.984 -11.43   0 0 2.540   1.19380     $inactive length
35 RCC  -12.7  1.984  8.890   0 0 2.540   1.19380     $inactive length
36 RCC  -12.7  1.984 -11.43   0 0 2.540   1.19380     $inactive length
37 RCC  -12.7  5.953  8.890   0 0 2.540   1.19380     $inactive length
38 RCC  -12.7  5.953 -11.43   0 0 2.540   1.19380     $inactive length
39 BOX  -16.51 8.900 -11.43   26.035 0 0   0 5.08 0   0 0 22.86
40 BOX  -16.51 -13.97 -13.97   26.035 0 0   0 27.94 0   0 0 2.54
41 RCC   0 0 -3.81   0 0 15.24   3.81
42 RCC   0 0 -10.666   0 0 2.33345133   5.4356       $Pu cylinder
43 PZ   -8.33254867                                  $Pu cylinder
44 BOX  -16.51 -8.89 11.43   7.62 0 0   0 17.78 0   0 0 2.54
45 PZ   11.43
46 PZ  -11.43
47 PX   8.89
48 PX  -8.89
49 PY   8.89
50 PY  -8.89
51 BOX -22.51 -17.31 -11.43   46.02 0 0   0 34.32 0   0 0 -5.08 $Poly

c     - data cards -
mode n
print
sdef   pos=0 0 -9.499274335 par=sf axs=0 0 1 rad=d2 ext=d3
si2    0 5.4356
si3   -1.166725665 1.166725665
fq0   e t f
f4:n  10 11 12 13 t
fm4   -1 13 103
sd4    1 1 1 1 1
t4     450 6850 1E12
f14:n ((10 11 12 13) < 24)
fm14   -1 13 103
sd14    1
f24:n ((10 11 12 13) < 25)
fm24   -1 13 103
sd24    1
f34:n ((10 11 12 13) < 26)
fm34   -1 13 103
sd34    1
f44:n ((10 11 12 13) < 27)
fm44   -1 13 103
sd44    1
f8:n  10 11 12 13 t
ft8   cap 2003
f18:n  (10 11 12 13)
ft18  cap 2003 gate 450 6400
c     t4   300 1100 1900 3500 6700 13100
```

```
m11    6000.66c 0.333 1001.60c 0.667    $HDPE density=0.96 g/cm3
mt11   poly.01t
m12   13027.66c 1.000                   $Al   density=2.70 g/cm3
m13    2003.66c 1.000             $He-3,10 atm,den=2.4463e-4 at/barn-cm
m14    8016.66c 0.210 7014.60c 0.790    $air
m15   14000.60c 0.334 8016.60c 0.666    $glass
m16   94238.66c -0.00048891
      94239.66c -0.72910337
      94240.66c -0.14524399
      94241.66c -0.00412629
      94242.66c -0.00306266
      95241.66c -0.00846288
       8016.66c -0.11797470
c      1001.66c -0.0011079044           $Pu mix sample
m17   26000.55c 1                       $Iron box
m18   98252.66c 1.000                   $Cf-252 source density 10e-20
nps   1000000
```

VITA

Angela Lynn Thornton received her Bachelor of Science degree in Nuclear Engineering from Texas A&M University in 2005. She entered the Nuclear Engineering graduate program at Texas A&M University in August 2005, and received her Master of Science degree in December 2007. Her research interests include nuclear non-proliferation, nuclear safeguards, and nuclear counterterrorism.

Ms. Thornton may be reached at 11123 Sagewind, Houston, TX, 77089 or by email at athorn@tamu.edu.